AD-A060 202 UNITED TECHNOLOGIES RESEARCH CENTER EAST HARTFORD CONN F/G 21/5
RESEARCH ON CENTRIFUGAL EFFECTS ON TURBINE ROTOR BLADE FILM COO--ETC(U)
AUG 78 R P DRING, M F BLAIR, H D JOSLYN F33615-77-C-2068
UNCLASSIFIED UTRC/R78-912944-7 AFAPL-TR-78-63 NL

1 OF 1
AD A060 202

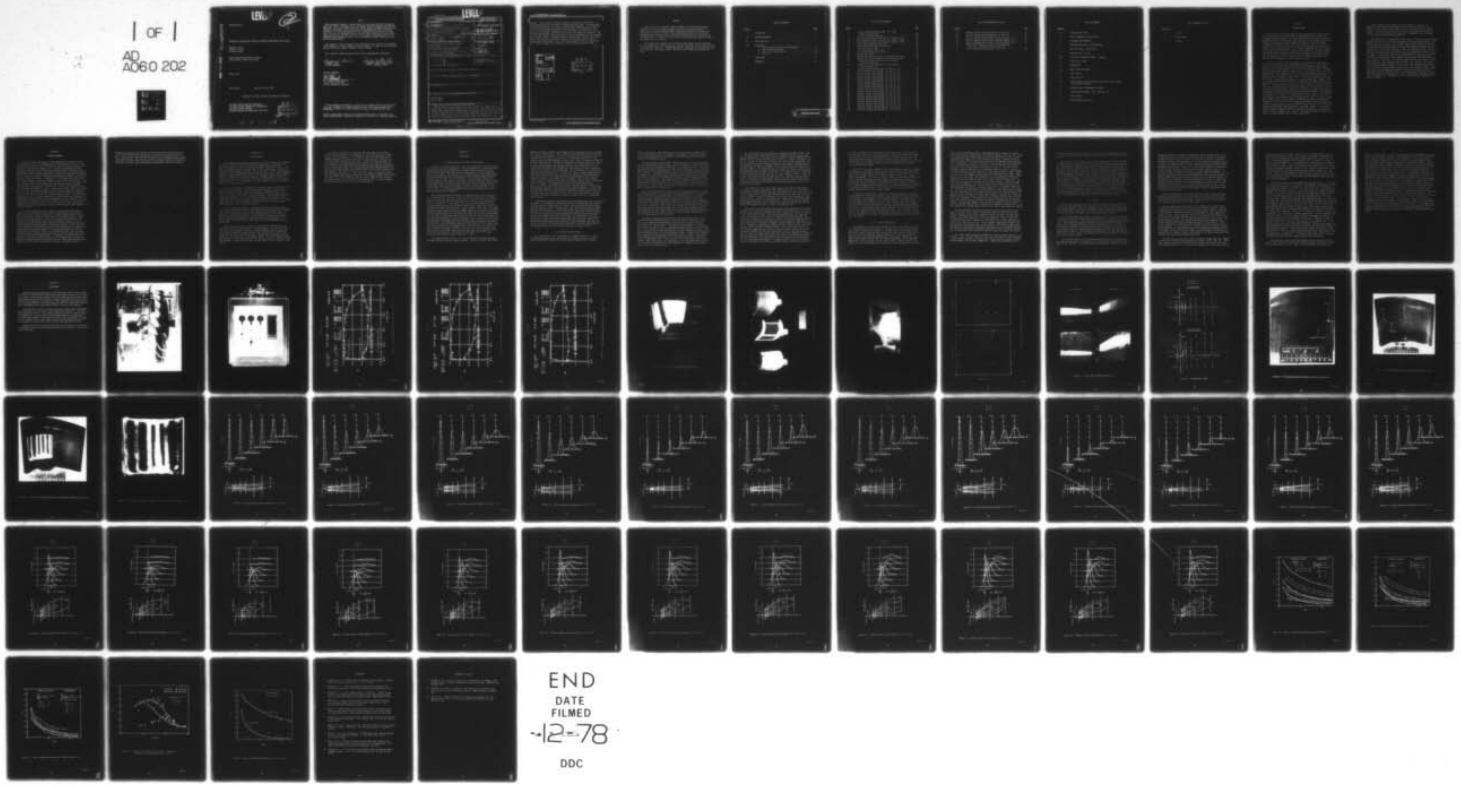

END
DATE FILMED
12-78
DDC

AFAPL-TR-78-63

RESEARCH ON CENTRIFUGAL EFFECTS ON TURBINE ROTOR BLADE FILM COOLING

Robert P. Dring
Michael F. Blair
H. David Joslyn

United Technologies Research Center
East Hartford, Connecticut 06108

August 1978

Final Report May 1977 to July 1978

AIR FORCE AERO PROPULSION LABORATORY
AIR FORCE WRIGHT AERONAUTICAL LABORATORIES
AIR FORCE SYSTEMS COMMAND
WRIGHT-PATTERSON AIR FORCE BASE, OHIO 45433

NOTICE

When Government drawings, specifications, or other data are used for any purpose other than in connection with a definitely related Government procurement operation, the United States Government thereby incurs no responsibility nor any obligation whatsoever; and the fact that the government may have formulated, furnished, or in any way supplied the said drawings, specifications, or other data, is not to be regarded by implication or otherwise as in any manner licensing the holder or any other person or corporation, or conveying any rights or permission to manufacture, use, or sell any patented invention that may in any way be related thereto.

This report has been reviewed by the Information Office (OI) and is releasable to the National Technical Information Service (NTIS). At NTIS, it will be available to the general public, including foreign nations.

This technical report has been reviewed and is approved for publication.

KERVYN D. MACH
Project Engineer

JOSEPH C. HURST, Major, USAF
Chief, Components Branch

FOR THE COMMANDER

H. I. BUSH, Deputy Director
Turbine Engine Division
AF Aero Propulsion Laboratory

"If your address has changed, if you wish to be removed from our mailing list, or if the addressee is no longer employed by your organization please notify AFAPL/TBC *,W-PAFB, OH 45433 to help us maintain a current mailing list".*

Copies of this report should not be returned unless return is required by security considerations, contractual obligations, or notice on a specific document.

UNCLASSIFIED

SECURITY CLASSIFICATION OF THIS PAGE (When Data Entered)

LEVEL II

REPORT DOCUMENTATION PAGE

READ INSTRUCTIONS BEFORE COMPLETING FORM

1. REPORT NUMBER: AFAPL-TR-78-63	2. GOVT ACCESSION NO.
3. RECIPIENT'S CATALOG NUMBER	
4. TITLE (and Subtitle): Research on Centrifugal Effects on Turbine Rotor Blade Film Cooling.	5. TYPE OF REPORT & PERIOD COVERED: Final, May 1977-July 1978
6. PERFORMING ORG. REPORT NUMBER: R78-912944-7	
7. AUTHOR(s): Robert P. Dring, H. David Joslyn, Michael F. Blair	8. CONTRACT OR GRANT NUMBER(s): F33615-77-C-2068
9. PERFORMING ORGANIZATION NAME AND ADDRESS: United Technologies Research Center, Silver Lane, East Hartford, Connecticut 06108	10. PROGRAM ELEMENT, PROJECT, TASK AREA & WORK UNIT NUMBERS: 3066-06-35
11. CONTROLLING OFFICE NAME AND ADDRESS: U.S. Air Force Aero-Propulsion Laboratory (TBC), Air Force Systems Command, Wright-Patterson Air Force Base, Ohio 45433	12. REPORT DATE: August 1978; 13. NUMBER OF PAGES: 63
14. MONITORING AGENCY NAME & ADDRESS (if different from Controlling Office)	15. SECURITY CLASS. (of this report): Unclassified; 15a. DECLASSIFICATION DOWNGRADING SCHEDULE

16. DISTRIBUTION STATEMENT (of this Report)

Approved for public release; distribution unlimited.

17. DISTRIBUTION STATEMENT (of the abstract entered in Block 20, if different from Report)

18. SUPPLEMENTARY NOTES

19. KEY WORDS (Continue on reverse side if necessary and identify by block number)

Turbine Blade
Film Cooling

20. ABSTRACT (Continue on reverse side if necessary and identify by block number)

Film cooling has been studied on the rotor blade of a large scale (low speed) model of a high pressure turbine first stage. Film coolant was discharged from single holes on the pressure and suction surfaces of the airfoil. For each blowing site the coolant-to-free stream mass flux ratio and density ratio were varied from 0.5 to 1.5 and from 1.0 to 4.0 respectively. Both surface flow visualization and local film cooling effectiveness data were

DD FORM 1 JAN 73 1473 EDITION OF 1 NOV 65 IS OBSOLETE
S/N 0102-LF-014-6601

UNCLASSIFIED

SECURITY CLASSIFICATION OF THIS PAGE (When Data Entered)

AD A059252

obtained. Film coolant effectiveness data is presented in the form of effectiveness profiles and contours downstream of each hole. The observation was made that although it can have a strong radial component, the trajectory of the film coolant was very insensitive to coolant flow conditions. The existence of the radial component of the film coolant trajectory was found to have a strong impact on the nature of the effectiveness distributions. The data have been compared with data taken by other investigators on flat surfaces and in plane cascades. Agreement between the flat plate data and the suction surface data was reasonably good. However, the pressure surface results showed a much faster decay of the effectiveness than did the flat plate data due to effects thought to be related to both curvature and radial flow.

PREFACE

This is the final technical report prepared by the United Technologies Research Center on a program sponsored by the Air Force Aero-Propulsion Laboratory, Air Force Systems Command, Wright-Patterson Air Force Base, Ohio, under Contract F33615-77-C-2068. This program was supported by the Turbine Components Branch and was under the technical direction of Dr. Kervyn Mach and Mr. Wayne Tall. Dr. Robert P. Dring of the United Technologies Research Center was responsible for the work.

The authors are indebted to the efforts of many people for the completion of this program and in particular to Mr. Charles Coffin for his skill and patience in building the models, Mr. Raymond Whitmore for developing the TC scanning system, and finally Mr. Joel Wagner and Mr. John Kostic for helping in acquiring the data.

TABLE OF CONTENTS

LIST OF ILLUSTRATIONS

LIST OF ILLUSTRATIONS (cont'd)

LIST OF SYMBOLS

Symbols

B_x	Airfoil axial chord
C_x	Axial component of flow velocity
D	Discharge hole diameter
I	Momentum flux ratio: $(\rho V^2)c/(\rho V^2)_f$
M	Mass flux ratio: $(\rho V)_c/(\rho V)_f$
R	Density ratio: (ρ_c/ρ_f)
Re_D	Blowing site Reynolds number: $(\rho_f V_f D/\mu)$
S	Surface arc length
T	Temperature
U_m	Wheel speed at midspan
V	Flow velocity
X	Axial distance
β	Angle between the discharge hole axis and a plane tangent to the airfoil surface
δ^*	Boundary layer displacement thickness
η	Cooling effectiveness: $(T_s - T_f)/(T_c - T_f)$
ρ	Fluid density
μ	Fluid absolute viscosity

Subscripts

c	Coolant
f	Free Stream
s	Surface

SECTION I

INTRODUCTION

With the evolution of gas turbine cycles with higher and higher turbine inlet temperatures has come the need for increasingly effective means of cooling the turbine airfoils. One such cooling technique currently receiving wide application is film cooling. The objective is to discharge a protective blanket of cooling air onto the surface of the airfoil with the purpose of insulating the airfoil from the hot flow around it. The film of air is created by injecting cooling air into the airfoil boundary layer through rows of holes on the airfoil surface. In its range of applicability film cooling offers numerous advantages over other cooling techniques. In higher temperature applications it provides a more effective means of cooling than simple internal convective cooling. Also, it does not require the arrays of much smaller diameter holes used in the "multihole" cooling schemes which are employed for even higher cooling effectiveness levels.

It is a curious fact that the feature of turbomachinery which makes it unique relative to most other fluid mechanical devices is rotation and yet it is this very feature which has historically received the least amount of attention. This is particularly true in the area of film cooling. Although film cooling has been applied to many turbine rotor blades, there is no background at all on the impact of rotation on the film coolant trajectory or film effectiveness. The potential exists for a relatively strong effect due to rotation since the density of the coolant fluid can be as high as three times that of the free stream fluid around it. During recent years, however, most of the other parameters affecting film cooling have been the subject of much careful scrutiny. A survey of work up to 1971 has been published by Goldstein (Ref. 1). Although the bulk of the discussion is related to slot injection, there was some discussion of isolated hole injection. Ericksen (Ref. 2) investigated film cooling behind a row of inclined holes, and among other things found that the effect of Reynolds number was relatively small. A simple analytical model of the effectiveness pattern produced by a jet has been published by Ericksen et al., (Ref. 3). Pedersen (Ref. 4) also looked at a row of inclined holes including mainstream to coolant density ratio as a prime variable. This permitted him to vary the mass and momentum flux ratios independently. He presented a correlation of his results including the effects of all these variables. Liess, et al., (Ref. 5) examined the effects of free stream acceleration and Mach number and found them to be small. Lander, et al., (Ref. 6) measured film cooling effectiveness on a first vane cascade in an attempt to include realistic geometry and flow conditions (including free stream turbulence). Finally, Muska, et al., (Ref. 7) confirmed the additive nature of the effectiveness of multiple rows of film cooling holes.

In the absence of any information on the effects of rotation, the assumption in the typical design system is that there is no effect. Rotor blades are treated like stator vanes in that it is assumed that the radial velocity in the film is zero and that the film follows the free stream flow around it. Any shortcoming of this approach is compensated for by calibrating the design system on engine experience.

Although there is no information on the impact of rotation on film cooling, there have been several studies on the effect it has on boundary layers. The analysis by Horlock, et al., (Ref. 8) addressed a particular set of similar laminar flows on a rotating helical blade. Their results indicated that even in a uniform density fluid significant radial flow could occur under certain circumstances in a boundary layer as a result of centrifugal forces. A recent analysis by Hules (Ref. 9) has indicated that for compressible turbulent boundary layers on rotor blades under most circumstances the radial flow is generally small. In preparation for the present program, an investigation was conducted into the nature of the boundary layer equations for stratified flow on a rotating curved blade. This analysis qualitatively confirmed the results described above. The equations indicated that in the regions of the blade surface where the free stream velocity is high (e.g., on the suction surface) the centrifugal effects are small, even for very dense boundary layers. However, in low free stream velocity regions (e.g., the pressure surface, separation bubbles and the stagnation region) the radial velocities are of the same order as the through-flow velocity, and consequently centrifugal effects would be expected to be significant. This is an important consideration since film cooling holes are frequently located in the low velocity region of the pressure surface.

SECTION II

PROGRAM BACKGROUND

One of the primary variables in this program was the coolant to free stream density ratio. This parameter was to be varied from 1.0 to 4.0. For this purpose the coolant fluid consisted of mixtures of air and sulfur hexafluoride, SF_6 (molecular weight = 146). SF_6 has the advantage of being chemically inert and also of having a high vapor pressure (320 psig @70° F). Measurement of both surface concentration of gas species (as done by Pedersen, Ref. 4) and surface temperature had been considered as a means of determining film coolant effectiveness. Temperature measurement was chosen for reasons of accuracy, speed, and expense. Furthermore, it was expected that this technique would provide an accurate simulation of the actual flow processes. This conclusion was based on the expectation that across the airfoil boundary layer the turbulent Prandtl number (governing heat transfer) and the turbulent Schmidt number (governing mass transfer) vary in such a way that their ratio, the turbulent Lewis number is close to unity at all points. This can be shown to be true for turbulent plane wakes from the results presented by Reynolds (Ref. 10, Figs. 4 & 5) and although there are basic differences in the flow, we expect the same to be true in a turbulent boundary layer. The mixtures were heated above the free stream temperature and effectiveness was determined by measuring the free stream and coolant temperatures and the adiabatic recovery temperature distribution on the airfoil surface with a matrix of thermocouples downstream of each blowing site. The airfoil was made of low conductivity urethane foam in order to minimize thermal conduction losses and to approach an adiabatic surface.

In order to investigate the full potential for radial flow effects to influence film coolant trajectory a number of blowing sites were selected. Hole locations were chosen at midspan at 10 percent axial chord on the suction surface and at 16 percent axial chord on the pressure surface. These holes are sufficiently far aft so as to be relatively uninfluenced by the details of the leading edge flow, and yet far enough forward so as to be uninfluenced by the suction surface endwall vortices and by the strong acceleration toward the trailing edge on the pressure surface. At the two locations selected the local flow velocity on the suction surface is roughly five times that on the pressure surface. It was expected that at the low free stream velocity locations, such as on the pressure surface, that the radial flow effects would be much more strongly felt than on the high velocity locations, such as on the suction surface. In addition, six other holes were provided. Since these entailed no delay to the program and only slight cost they were included in areas of possible interest. These additional holes are near the tip at 50 and 75 percent axial chord on the pressure surface, at

midspan at 40 percent and 65 percent on the suction surface and at 60 percent on the pressure surface and near the root at 16 percent on the pressure surface. These six additional blowing sites were only incorporated into the flow visualization models. They were not included in the instrumented effectiveness test models which were fabricated later in the program. Because of scheduling constraints, however, these six additional blowing sites were never tested.

SECTION III

TEST FACILITIES

The experimental program was carried out in the UTRC Large Scale Rotating Rig (LSRR). This facility is five feet in diameter and is shown with the partially assembled 0.8 hub/tip ratio turbine model installed in Fig. 1. At a typical running condition, the axial flow velocity in the rig is 75 f/s (23 m/s) and the shaft speed is 405 rpm. The airfoil axial chords are typically 6 inches, (0.15 m) or approximately five times the engine scale. Airfoil Reynolds numbers are approximately 5.6×10^5 which is typical of high pressure turbine airfoils. Because the rig also has velocity triangles typical of those of a high pressure turbine, it provides an excellent simulation of the centrifugal and Coriolis effects as they would occur in the boundary layers of an actual engine scale turbine airfoil.

The rig is operated by a computerized automatic control, data acquisition and data reduction system. This system precisely maintains the desired rig velocity triangles (C_x/U_m), acquires all pneumatic and thermocouple data and reduces this data (on-line) to engineering units and to convenient dimensionless parameters. The system includes automatic calibration procedures for all pneumatic transducers. For the present program this system was used to acquire the rotor airfoil pressure distribution data and the rotor film cooling temperature data. The system also converted these data to pressure coefficients and film coolant effectiveness ratios.

A flow metering system was assembled and calibrated to provide precise flows of the film coolant fluid to the blowing sites at various coolant blowing rates (M) and various coolant to free stream fluid density ratios (R). As previously discussed, the coolant flow consisted primarily of a mixture of sulfur hexafluoride (SF_6) and air. A trace amount of ammonia was included for flow visualization purposes. Mixtures of air and SF_6 permitted the entire range of coolant flow rate and coolant to free stream density ratio to be obtained.

The flow metering system, consists of three Matheson 150 mm glass tube flow meters and one Fischer-Porter 1/2 inch flow meter. For each gas to be used (SF_6, air and ammonia) there is a separate plumbing circuit consisting of a pressure regulator, needle valves at the inlet and outlet of the flow meter body and a precision pressure gage. Glass tubes for various flow rate ranges may be inserted into the flow meter frames. The various gages, valves, and flow meters can be seen on the face of the unit in Fig. 2. The three flows are combined in a union and then pass into the turbine airfoil through a rotary union.

In order to accurately set flows over the wide range of flow rates required, the flow meters were calibrated with glass tube and float combinations of various capacities. The flow meter tube/float combinations were calibrated against a Precision Scientific Co. Wet Test Meter using the specific gas for which they were to be used. Calibrations were performed at 0, 20, and 60 psig. The high pressure was required to overcome the line pressure drop that occurred between the flow metering system and the blowing site on the turbine rotor blade. The calibrated glass tubes (Matheson models 601, 602, 603, 604, and 605 and Fischer-Porter model 1/2-17-40 Float) provide flow rate ranges of $.05 \times 10^{-4}$ to 55×10^{-4} and $.015 \times 10^{-4}$ to 30×10^{-4} lbm/sec, respectively for SF_6 and air. Since only trace amounts of ammonia were necessary, the ammonia meter was calibrated only with a Matheson model 601 tube from $.01 \times 10^{-4}$ to 0.1×10^{-4} lbm/sec. Over the entire range the error expected from these meters is $\pm$ 1 1/2 percent on the average and $\pm$ 3 percent maximum. This was more than sufficient for the intended testing.

SECTION IV

DISCUSSION

A. Blade Pressure Distribution Measurements

In order to set the coolant flow rate, it was necessary to know the free stream velocity at each blowing site. For this purpose the rotor blade midspan pressure distribution was measured at a nominal (design) value of (C_x/U_m) of 0.78 and at higher and lower values corresponding to plus and minus five degrees of incidence. The incidence was changed by varying rotor speed (holding flow constant) and hence the blade axial chord Reynolds number remained constant (at 5.6×10^5) for all incidences. The data taken included (1) airfoil midspan surface pressures at twenty-two locations around the perimeter of the blade, (2) rotor inlet relative total pressure at midspan (from a rotor mounted Kiel probe) and (3) rotor exit tip static pressure measured on the rotor casing. The pressure instrumented airfoil can be seen mounted on the rotor in Fig. 1. The rotating frame pressures were measured using a rotor-mounted scanivalve and transducer.

When comparing measured pressures to computed pressure distributions, it is convenient to use a pressure coefficient based on the blade exit midspan static pressure as a reference pressure and the difference between the blade inlet total pressure and the midspan exit static pressure as a normalizing pressure difference. It was found in all cases that the measured pressure surface maximum pressures were slightly lower than one would expect from the measured rotor inlet total pressures. This difference, however, is only about 1 percent of the rotor exit relative dynamic pressure. This effect is probably related to radial flows in the rotor channel shifting the location of the high and the low total pressure fluid between the inlet total pressure probe (which is at the rotor leading edge plane) and the 30 percent chord location where the pressure surface pressure is near its maximum. In all cases the total pressure that was inferred from the pressure surface was used in evaluating the airfoil distributions. The midspan exit static pressure was determined by applying a correction to the static pressure measured on the rotor exit tip casing. This correction was based on the assumption of free-vortex flow. This is a very small correction (roughly 1 percent of the rotor exit relative dynamic pressure) and hence the slight inaccuracy associated with the assumption of free-vortex flow is negligible. The results for the three values of (C_x/U_m) tested are shown as data points in Figs. 3, 4, and 5.

The computed curves in Figs. 3, 4, and 5 are based on an existing UTRC developed inviscid potential flow calculation. The inlet and exit flow angles

(BETA1D and BETA2D, measured from tangential) were adjusted to give best agreement with the measurements. Notice that excellent agreement has been achieved at a nominal inlet angle of 41° and at plus and minus five degrees for the low and high values of (C_x/U_m) respectively. A single exit angle (25.5°) was shown to give excellent agreement for all cases. These flow angles are also in excellent agreement with a meanline analysis which had been carried out earlier for this turbine model. The flow was assumed to be incompressible (M1 = M2 = 0) since the Mach number levels reached in the rig are less than 0.2. The stream tube contraction ratio (H2/H1) was taken from an existing through-flow analysis of the flow in the turbine model. As can be seen, it is very close to unity at this midspan location. The loss has only a relatively weak impact on the pressure distribution, but in order to be complete, a span-averaged loss value was included. This value had been measured by UTRC during an earlier program in the rig at the design value of (C_x/U_m). This loss was assumed to be a constant fraction of the rotor exit relative dynamic head at off-design values of (C_x/U_m). The definition of the pressure coefficient used in Figs. 3, 4, and 5 is included on the figures. As mentioned previously, it is based on the inlet total pressure and the exit static pressure. The predicted trailing edge stagnation point singularity has been eliminated in favor of the more physically realistic trailing edge condition of a base pressure equal to the downstream static pressure ($C_p = 0$). This affects the pressure distribution over less than the aft-most 10 percent of the airfoil, i.e., from X/BX from 0.9 to 1.0.

In general the measured and computed pressure distributions are in excellent agreement. The agreement is especially good in the leading edge region where the film coolant blowing sites are located. The suction and pressure surface blowing sites are 10 and 18 percent axial chord respectively from the leading edge as indicated in Fig. 3. From these results it has been determined that the local surface flow velocities at the suction and pressure surface blowing sites are (as a fraction of rotor midspan wheel speed) 2.05 and 0.40 respectively at the design point value of (C_x/U_m). This corresponds to 196 and 38 feet per second at a typical running condition of 405 rpm. These results were used to compute the various film coolant mass flow rates required to achieve the desired values of the coolant to free stream mass flux ratio (M) and the coolant to free stream density ratio (R). From this point onward all testing was carried out only at the design value of $(C_x/U_m = 0.78)$.

B. Flow Visualization Tests

The first phase of the film cooling test program consisted of a series of flow visualization tests. The objective of these tests was to qualitatively determine the nature of the film coolant footprint on the airfoil

surface downstream of each blowing site for the full range of density ratios (R) and blowing rates (M) to be studied in the program. These flow visualization film cooling patterns could then be employed to determine the effectiveness instrumentation arrays.

The same procedure was employed to fabricate both the flow visualization and effectiveness test blades. Holes, (1/8 inch diameter, 3.2 mm) were drilled into an existing aluminum rotor blade (B_x = 6.34 inches, 16.1 cm). The hole locations are known to within 0.3 percent of axial chord which is a relatively small fraction of the hole diameter. Each hole is inclined at an angle of 30^o to the surface. The plane of each hole was set such that the axis of the hole is tangent to a cylindrical surface intersecting the airfoil at the location. The result is that all of the holes are oriented in the streamwise direction with no radial component. The rather complicated angular orientations of the holes were carried out with high precision by mounting the airfoil on a sine plate which in turn was mounted on a jig boring machine. The final result is shown in Figs. 6 and 7 where pins have been inserted into each of the holes to better illustrate their orientation.

A mold was then fabricated using the drilled aluminum airfoil as a master. The blade was mounted in a jig using the hub attachment button as a location guide. A frame was placed around the airfoil and a ground drill rod was inserted into the eight holes in the airfoil through holes in the frame. Parting surfaces were made along the leading and trailing edges with special care taken at the leading edge where a smooth joint between the two mold halves is critical. Hydrocalic cement was used to cast around the metal master with the drill rods inserted. This cement has extremely low shrinkage so that the final mold shape is an accurate duplicate of the original aluminum airfoil. Upon hardening, the drill rods and the metal airfoil were removed and the mold was allowed to cure for a week. Finally, the mold surface was polished to ensure a smooth model with a clean skin.

In order to provide structural integrity to the final airfoil, a steel skeleton was fabricated consisting of a hub attachment button identical to that of the original aluminum airfoil, two steel airfoil shaped sections located near the root and tip of the blade and three spanwise steel spars. This skeleton is shown in Fig. 7. The skeleton was mounted by its hub attachment in the locating jig and the mold halves brought together. The drill rods were reinserted into the mold and connected to geon tubing which passed out of the mold through holes in the hub attachment button. Urethane foam (Isofoam^R, Witco Chemical) was poured into the mold and allowed to harden. This particular foam material was selected for its extremely low thermal conductivity (0.02 to 0.03 Btu/hrft ^oF). This is nearly as low as the value for still air (0.014). While this property is unimportant to the flow visualization tests, it is a crucial consideration for the measurement of adiabatic wall temperatures in the effectiveness tests.

The final results of this fabrication procedure are shown in Figs. 7 and 8. Two airfoils were fabricated with four individual blowing sites on each. The two blowing sites of principle interest, namely, those at midspan near the leading edge on the pressure and suction surfaces, are both on the airfoil in Fig. 8. One hole on the suction surface can be seen in this photograph. The final cast models are near perfect replicas of the original aluminum airfoil. The surface of the model is composed of a very thin skin of urethane which is extremely smooth. The leading edge is also virtually flawless. Special care was taken here since, as mentioned above, this was the location of the parting surface between the two halves of the mold. The intersections of the various blowing holes with the airfoil surface are also virtually flawless. Each one is very clean without either flat spots or burrs. Finally, care was taken to insure that each hole had a straight length of at least four diameters (1/2 inch, 1.3 cm) before it entered the geon tube within the model. This insured an adequately uniform and developed flow discharging from each hole at the surface of the airfoil.

Upon completion of the rotor blade pressure distribution measurements, the two flow visualization airfoils were installed in the rig. The suction and pressure surface blowing sites, were each connected to one channel of a two channel rotary union. The gas flow metering device was connected to either of the two channels so that both blowing sites could be run in sequence during a single rig run. A piece of ozalid paper was cemented onto each airfoil immediately behind the hole at each blowing site. The airfoils had been marked with spanwise reference lines so that all the pieces of ozalid paper mounted behind each blowing site were in exactly the same position.

With a piece of ozalid paper mounted behind each blowing site the rig was brought up to the desired running conditions of thru-flow velocity (C_x) and midspan wheel speed (U_m) such that the nominal design point velocity triangles (i.e., C_x/U_m) were obtained. The flow metering device was then connected to one of the blowing sites and the air and sulfur hexafluoride (SF_6) flow rates were adjusted until the desired coolant to free stream density ratio (R) and coolant to mainstream mass flux ratio (M) were obtained. When the flow was established, a trace amount of ammonia was introduced into the film coolant flow. The amount of ammonia was always less than 1 percent of the total coolant mass flow so it had a negligible effect on both the R and M ratios. A strobe light triggered with a once per revolution pulse from the rotor shaft was used to observe the flow trace established itself on the ozalid paper. After a trace of suitable darkness had been achieved the ammonia was turned off and the lines were flushed with ammonia free flow. The flow metering device was then connected to the rotary union channel leading to the other blowing site and the process was repeated. As shown in Fig. 9, a matrix of R and M ratios was covered on both the suction and pressure surfaces corresponding to

the range of typical gas turbine film cooling applications. On the suction surface, high M ratios could not be obtained at low R ratios due to the large pressure drop occurring in the supply lines for this highest flow rate case. This problem was rectified in the effectiveness testing. However, it is not expected that any information was lost in the flow visualization since both the suction and pressure surface coolant trajectories appear to be virtually invariant with both R and M.

Figure 10 is a typical example of the flow visualization results. Traces are shown for a low M ratio and for both the suction and pressure surface blowing sites at nominal density ratios (R) of 1 and 4. In all cases the suction surface film coolant trajectory is narrow, straight and has only a slight radial displacement. The pressure surface trajectory on the other hand is much wider, displays noticeable curvature, and has a strong radial displacment (roughly 30^{o} radially outward). In comparing the various traces it must be kept in mind that the relative darkness of each trace is primarily a function of how long the ammonia was allowed to flow. It should not be related directly to film coolant effectiveness. The trace width is also a function of the ammonia flow time but to a much lesser degree.

In order to gain additional insight into the flow mechanisms occurring in the experiment, a very small amount of pure ammonia was passed through both blowing sites. It was expected that this would indicate the nature of the flow over the blade in the absence of film coolant discharge. The results were virtually identical to those of Fig. 10. This indicates that it is unlikely that the pressure surface radial flow is due to a three-dimensional boundary layer since if this were the case the flow visualization trace direction would be expected to change somewhat when going from very low to very high blowing rates as the coolant jet penetrated the free stream. Such a change in direction was not observed to occur. The suction and pressure surface film coolant trajectories appear to be simply following the three-dimensional inviscid flow over the airfoil.

C. Effectiveness Measurements

Upon completion of the flow visualization tests, the fabrication of the two instrumented effectiveness airfoils was initiated. The two airfoils were cast using the previously discussed low thermal conductivity urethane foam. One airfoil had the suction surface blowing site (at 10 percent chord) and the other airfoil had the pressure surface blowing site (at 16 percent chord). These airfoils were cast with thermocouples (TC's) mounted internally in the film coolant supply lines so that the coolant temperature could be measured immediately prior to ejection at the airfoil surface. The positions of the rows of TC arrays downstream of each blowing site were determined on the basis

of the flow visualization results. The diagrams used to locate the suction and pressure surface thermocouple (TC) arrays are shown in Fig. 11. The streamwise positioning, the radial extent and the locations where TC's were concentrated were all based on the flow visualization results. Figures 12 and 13 show the arrays on the airfoils with the suction and pressure surface blowing sites respectively. Six rows of hole pairs (two for each TC) can be seen with 8 to 12 thermocouples mounted in each array. The TC rows have been shown in relation to the airfoil pressure distribution in Fig. 3. In brief, the TC mounting procedure consisted of the following sequence of steps. A series of terminal strips (one for each row of TC's) were prepared with 1.2 meter lengths of 3 mil (.075 mm) diameter chromel-alumel wire pairs mounted on them. These wires carry the TC voltage from the airfoil to a rotating frame voltage scanner mounted on the rotor axis. The terminal strips were mounted in a recessed chamber cut into the opposite side of the airfoil from the blowing site. The lead wires are routed out through the blade hub attachment. Figure 14 shows the recessed chamber cut into the pressure surface of the airfoil having the suction surface blowing site. The hole pairs from the TC locations were then drilled through the airfoil to positions adjacent to the terminal strips (Fig. 15). One mil (.025 mm) diameter chromel-alumel TC's were then inserted through the holes and welded onto the chromel-alumel lead wires protruding through the terminal strips. When all of the TC's were mounted a thin coat of varnish was applied to the test surface to hold the TC's firmly in position and to restore the surface smoothness. The welded wires on the terminal strips were potted with a thin layer of epoxy to prevent any motion or breakage due to centrifugal loading. The recessed chamber in the airfoil was completely filled with the piece of urethane foam that had originally been removed to form the cavity. By this approach the original smooth contour of the airfoil was completely restored.

The instrumented airfoils were mounted on the rotor hub of the turbine model in the rig. The "coolant" fluid passed from the calibrated metering system, through a rotary union, through an electrical heater, and into each airfoil. The heater was used to bring the coolant gas flow to a temperature approximately 50° F above that of the mainstream fluid. The TC lead wires from both airfoils were connected to a 144 channel TC scanning system mounted on the rotor (near the rig axis). The TC scanner communicated digitally with the previously described rig data system computer. This digital communication eliminated all difficulties associated with slip-ring noise on analog signals. The "coolant" temperature was measured immediately prior to discharge from the airfoil surface by the TC's mounted inside the supply line within the airfoil.

The coolant supply system was designed to provide a coolant mixture to one blade at a time. For each flow condition, then, one blade was film cooled and the other blade provided a convenient and accurate station to measure the free stream adiabatic wall recovery temperature. Individual thermocouples on the

film-cooled blades were calibrated by recording indicated temperatures with no cooling air flowing. All TC calibration corrections were less than or equal to 0.5^{o} F.

The results of the testing on the suction and pressure surfaces for twelve combinations of M and R ratios on each surface are shown in Figs. 16 through 39. These figures illustrate the profiles across the film coolant footprint at each array of TC's. Sketched below them are isoeffectiveness contours that have been inferred from the profiles. Several thermocouples became inoperative during the final stages of model fabrication, during installation in the rig and during testing. In total, 6 out of the total of 130 TC's were inoperative. All of the bad TC's were on the suction surface and they have been indicated on Figs. 11 and 16 through 27. Due to this loss of instrumentation, some artistic license had to be employed in constructing the effectiveness profiles on the suction surface. In areas where this was done, the profiles have been drawn with dashed lines. In addition, since the uncertainty in the measured effectiveness is approximately $\pm$ 1 percent the locations of the 0.02 contours, and also, but to a lesser degree, the 0.05 contours, are not considered precise. For this reason, they have been drawn in as dashed lines in all of the figures. The degree to which most of the effectiveness profiles return to zero on either side of the footprints is indicative of the uncertainty in the results.

D. Results

The film cooling patterns obtained from the separate flow visualization and film effectiveness tests were consistent for all tests on both the suction and pressure surfaces. This was an important aspect of the test program since, as discussed above, the location and density of the effectiveness instrumentation was selected on the basis of the flow visualization results.

The effectiveness pattern (Figs. 16 through 39) can be seen to bear close resemblance to the flow visualization patterns (Fig. 10). The suction surface effectiveness footprint is narrow and has only a slight radially outward deflection. Even though the maximum effectiveness and the footprint width vary markedly over the range of M and R tested, the location of the centerline of the footprint appeared to be insensitive to these variables. As in the flow visualization tests, the pressure surface footprint was wide and exhibited a large radial deflection. The maximum effectiveness and the footprint width on the pressure surface, however, both appear to be far less sensitive to M and R than on the suction surface.

The different widths of the suction and pressure surface coolant patterns are somewhat analogous to the differences in film coolant coverage that can be achieved through the use of compound angled blowing holes as opposed to simple

streamwise blowing. A blowing configuration in which the major axis of the ellipse formed by the intersection of the hole and the surface is parallel to the main stream velocity of the flow over the hole is referred to as simple streamwise blowing. When the major axis of the ellipse is not parallel, it is referred to as compound angled blowing. Generally speaking, compound blowing can result in a much wider film coolant effectiveness footprint than simple streamwise blowing (Refs. 11 and 12). On the suction surface the major axis of the ellipse is parallel to the film coolant trace and the result is a relatively narrow trace which is typical of simple streamwise blowing. In contrast to this, the major axis of the pressure surface hole ellipse is at an angle of approximately 30^{o} to the film coolant trace and this has produced the much wider film coolant footprint characteristic of compound blowing. As mentioned in the discussion of the flow visualization tests, it appears that the film coolant trajectory is governed primarily by the nature of the undisturbed flow over the airfoil, i.e., in the absence of film cooling. Centrifugal and Coriolis forces may be important in determining the nature of the undisturbed flow, but beyond that, they appear to have no significant impact on film coolant trajectory.

The basic conclusions of the program are that there is a strong radial component to the pressure surface film coolant trajectory and that both the suction and pressure surface trajectories are very insensitive to both the density ratio (R) which was varied over a range from 1 to 4 and the mass flux ratio (M) which was varied over a range from 0.5 to 1.5.

The fact that film coolant trajectory is insensitive to coolant flow conditions eliminates one of the concerns of the turbine designer. However, one must keep in mind that the pressure surface coolant trajectory represents a wide departure from typical design system assumptions. This can give rise to two problems. First, large portions of the airfoil surface downstream (axially) of the coolant discharge hole will be starved of film coolant since this air will have moved radially outward toward the tip of the airfoil. The second problem arises in that compound angled holes are frequently used to achieve improved film cooling coverage on turbine airfoil surfaces. These holes are generally oriented under the assumption of purely axial flow on the airfoil surface. If the radial flow occurring on the blade pressure surface was aligned with the compound hole angle, the enhanced film coverage would not be achieved. The result of both of these possible problems would be burning near the airfoil pressure surface trailing edge in the region downstream of the blowing sites experiencing maximum radial flow.

The effectiveness data taken during the present program have been compared to flat plate wind tunnel data reported by Goldstein et al., (Ref. 11). There were, however, some differences between the present film cooling test conditions and those of Ref. 11. For the present program, the suction and pressure

surface holes are at 30° to the surface, but in the tests of Ref. 11, the holes were 35° from the surface. For the present program, the pressure and suction surface blowing site Reynolds numbers (Re_D) are 0.24 x 10^4 and 1.27 x 10^4, respectively, whereas for the tests of Ref. 11 values of 2.2 x 10^4 and 4.4 x 10^4 were employed. This difference is not believed to be important since the data of Refs. 1 and 5 indicate that film effectiveness is insensitive to Reynolds number. Most of the data reported in Ref. 11 are for a normalized displacement thickness (δ^*/D) of 0.116. For the present tests, (δ^*/D) is 0.036 and 0.059 on the suction and pressure surfaces respectively. The reduced coolant injection angle and (δ^*/D) ratio of the present tests would both be expected to produce effectivenesses slightly higher than those of Ref. 11. This generally did not turn out to be the case as shall become apparent in the following paragraphs.

The suction surface data are compared with the data of Ref. 11 in Fig. 40. For a density ratio (R) of 1.0 the decay of the maximum effectiveness is shown as a function of normalized distance aft of the center of the blowing site. For blowing rates (M) of 1.0 and 1.5, the present data are in reasonably good agreement with the data of Ref. 11. At M = 0.5, there is a significant difference. The reason for this difference is unclear at present, but it may be due to the effects of curvature as shall be discussed below. The pressure surface data are compared with the same flat plate data of Ref. 11 in Fig. 41. As can be seen, significant differences exist between the two sets of data for all conditions. The effectiveness data of the present program are, in general, much lower and less sensitive to M than those of Ref. 11. The pressure surface data, however, show a greater similarity to the data of Ref. 11 which were obtained with the hole oriented at right angles to the flow direction (Fig. 42). The lower level of maximum effectiveness and its relative insensitivity to M appear to be partially a result of the radial flow over the blowing site causing the hole to behave as a compound angled hole. A final comparison with the data of Ref. 11 is given in Fig. 43, where the maximum effectiveness is plotted as a function of the momentum flux ratio ($I = M^2/R$) at a normalized distance downstream of the hole center (S/D) of 6.6. Although the suction surface results are in reasonably good agreement with those of Ref. 11, the pressure surface results are distinctly different. The conclusion drawn from these comparisons is that although the suction surface film coolant behavior is similar in many respects to what one would have expected, based on the flat plate results of Ref. 11, the pressure surface results are both qualitatively different (i.e., a strong radial component to the coolant trajectory) as well as quantitatively different (i.e., the effectiveness levels are, in general, much lower than one would have expected from flat plate results).

The difference between the data presented here and those of Goldstein et al., (Ref. 11) may partially result from the effects of surface curvature. In a recent paper, Ito et al., (Ref. 13) have reported film cooling data

taken on a turbine blade in a plane cascade with rows of blowing sites on both the suction and pressure surfaces. Their holes were at 35° to the surface and had a center-to-center distance of three diameters. In all other respects, their configuration was very similar to that of the present program. Their facility being a plane cascade, however, had no radial flow effects. Most of the data they present is laterally averaged but some local effectiveness data is reported for a density ratio of 0.95 and a mass flux ratio of 0.5, for the pressure and suction surfaces. This data, on the hole centerlines.(Ref. 13, Figs. 4 and 5), is almost identical with that of the present program on the suction surface, and it is also quite close on the pressure surface (Fig. 44). The pressure surface effectiveness data of Ref. 13 are higher by 0.05 to 0.10 than those of the present program, a difference probably due to the effect of the row of holes as opposed to the single hole employed in the present program. Ito et. al., (Ref. 13) attribute most of the differences between suction and pressure surface film cooling behavior to the effects of surface curvature. The effects of high and low blowing rate and concave and convex surface curvature are summarized by Ito et al.(Ref. 13), in Fig. 10 of that work. This figure is for laterally averaged effectiveness, but it is similar in many respects to Fig. 43 of the present report. The high effectiveness on the suction surface at low momentum flux ratios (I) is attributed by Ito et al., to the effect of curvature causing the coolant jet to be close to the wall. At higher values of I, the curvature effects cause the jet to lift off the surface resulting in lower effectiveness. On the pressure surface, the effects were shown in (Ref. 13) to be reversed. Low values of I caused low effectiveness, but the effectiveness increased gradually as I increased. It was suggested by Ito et al., and indeed it is confirmed by their data as well as by that of the present report (Fig. 43), that the suction (convex) and pressure (concave) surface curves should cross at a value of I equal to or somewhat greater than unity.

SECTION V

CONCLUSIONS

Both qualitative and quantitative differences were seen to exist between the behavior of film coolant on the suction and pressure surfaces of a turbine rotor blade. On the suction surface, the film coolant had only a small radial displacement and was in many respects similar to existing data taken on flat surfaces with streamwise oriented holes. Where comparisons were possible, the suction surface data was also nearly identical with film cooling data taken by other investigators on a plane cascade airfoil of very similar geometry.

On the pressure surface, the film coolant had a large radial displacement and, in general, very low levels of effectiveness were measured. The radial displacement was a result of the radial component of the free stream flow over the blowing site. The low level of effectiveness appears to be due both to the effectively compound orientation of the hole, due to the radial flow, and surface curvature effects which tend to reduce coolant effectiveness on concave surfaces at momentum flux ratios (I) less than approximately unity.

Finally, the film coolant trajectories for each blowing site are virtually uninfluenced by the coolant blowing rate (M) and by the coolant to free stream density ratio (R).

(FIRST VANE AND ROTOR CASE REMOVED)

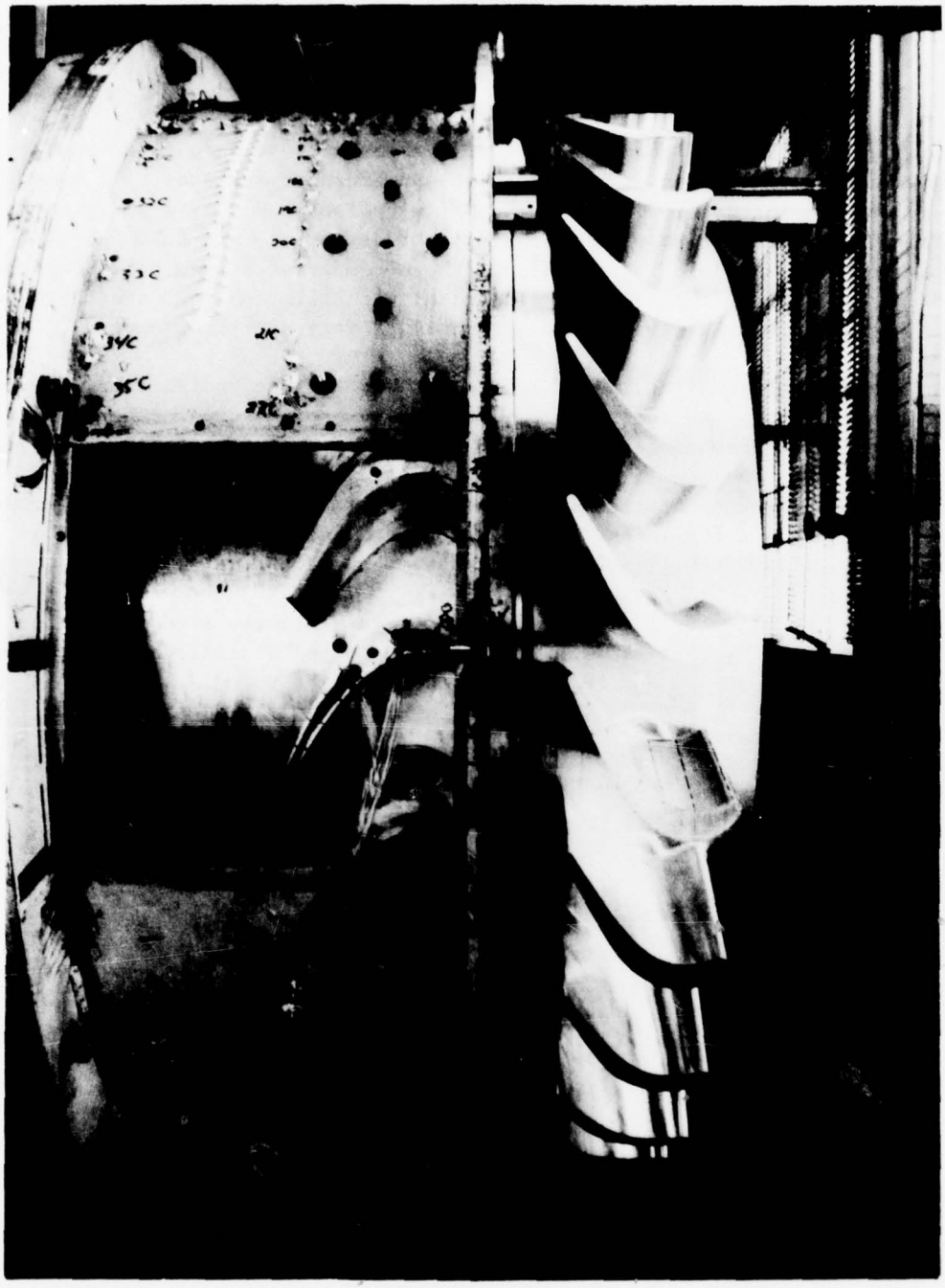

Figure 1. Large Scale Rotating Rig 1-1/2 Stage Turbine Configuration

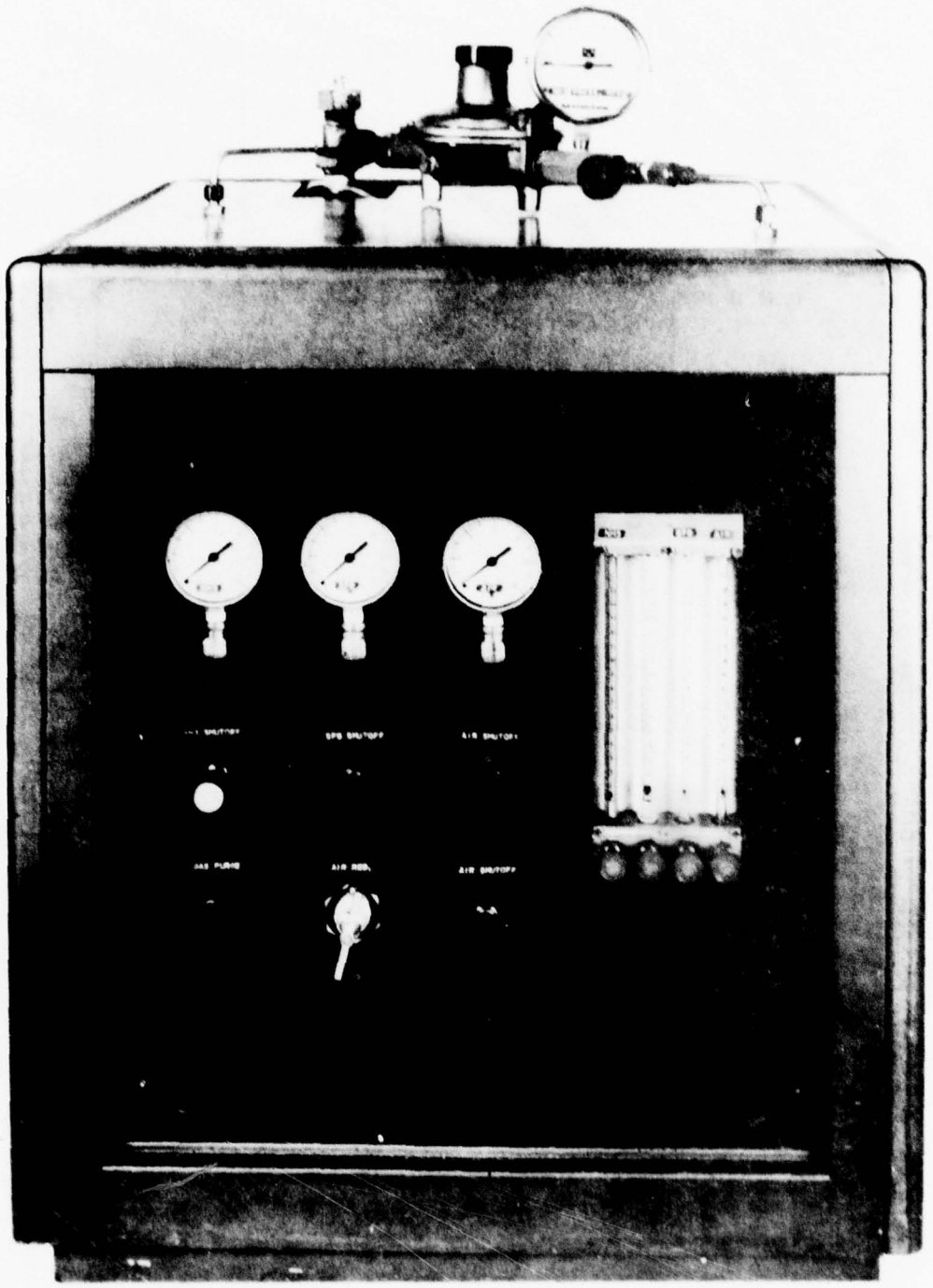

Figure 2. LCRR Coolant Flow Metering System

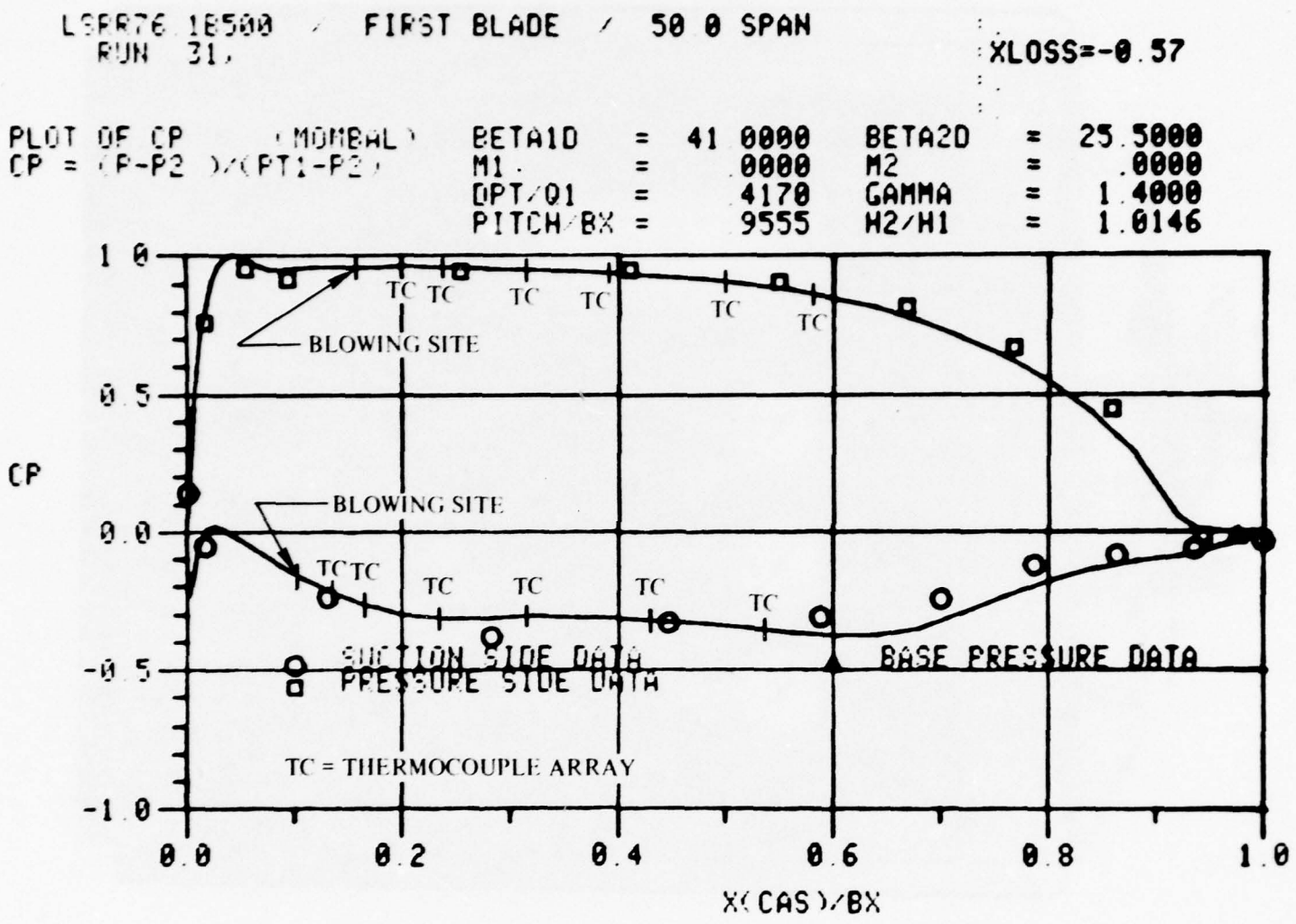

Figure 3. Rotor Midspan Pressure Distribution, $(C_x/U_m) = 0.78$

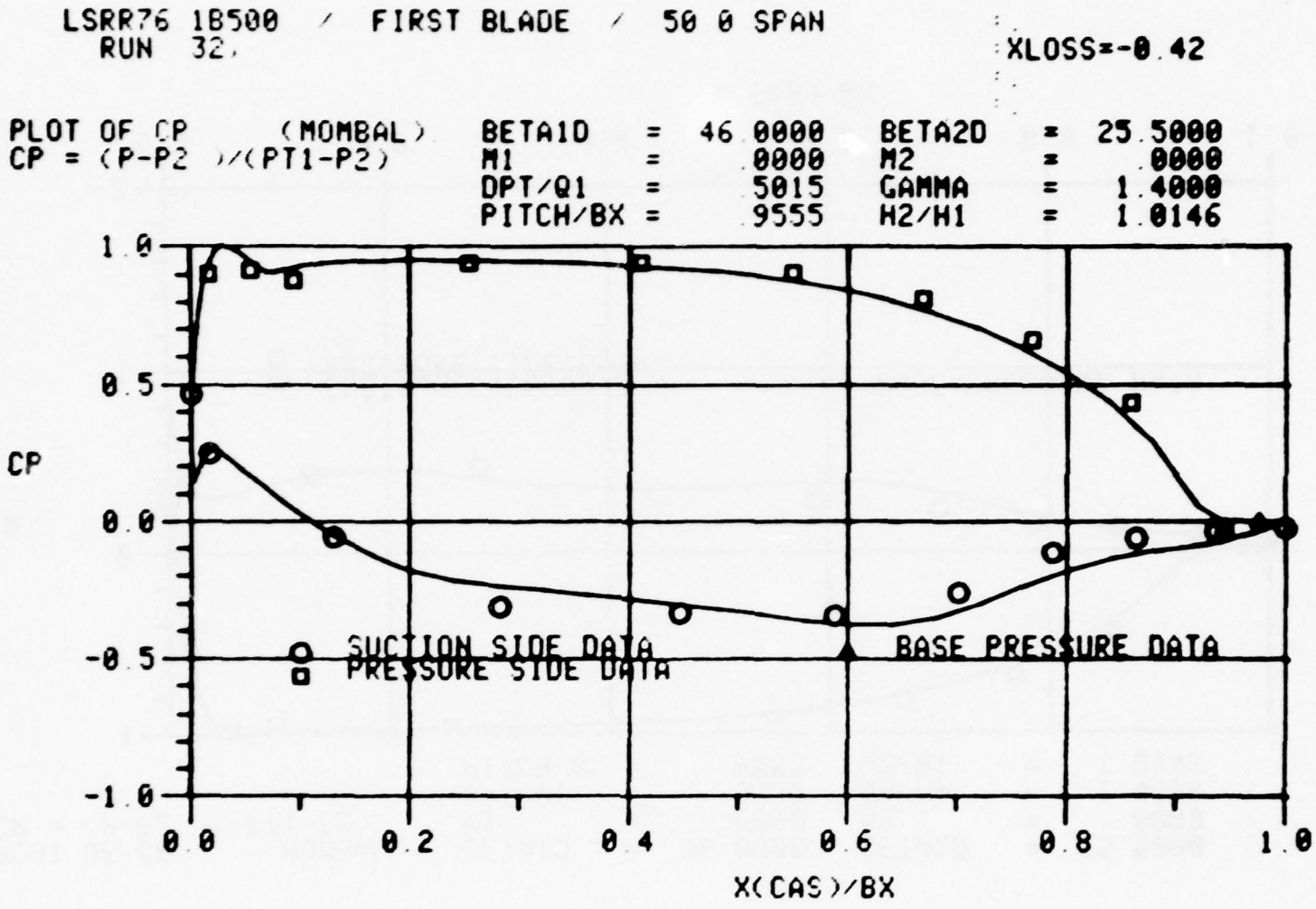

Figure 4. Rotor Midspan Pressure Distribution, $(C_x/U_m) = 0.68$

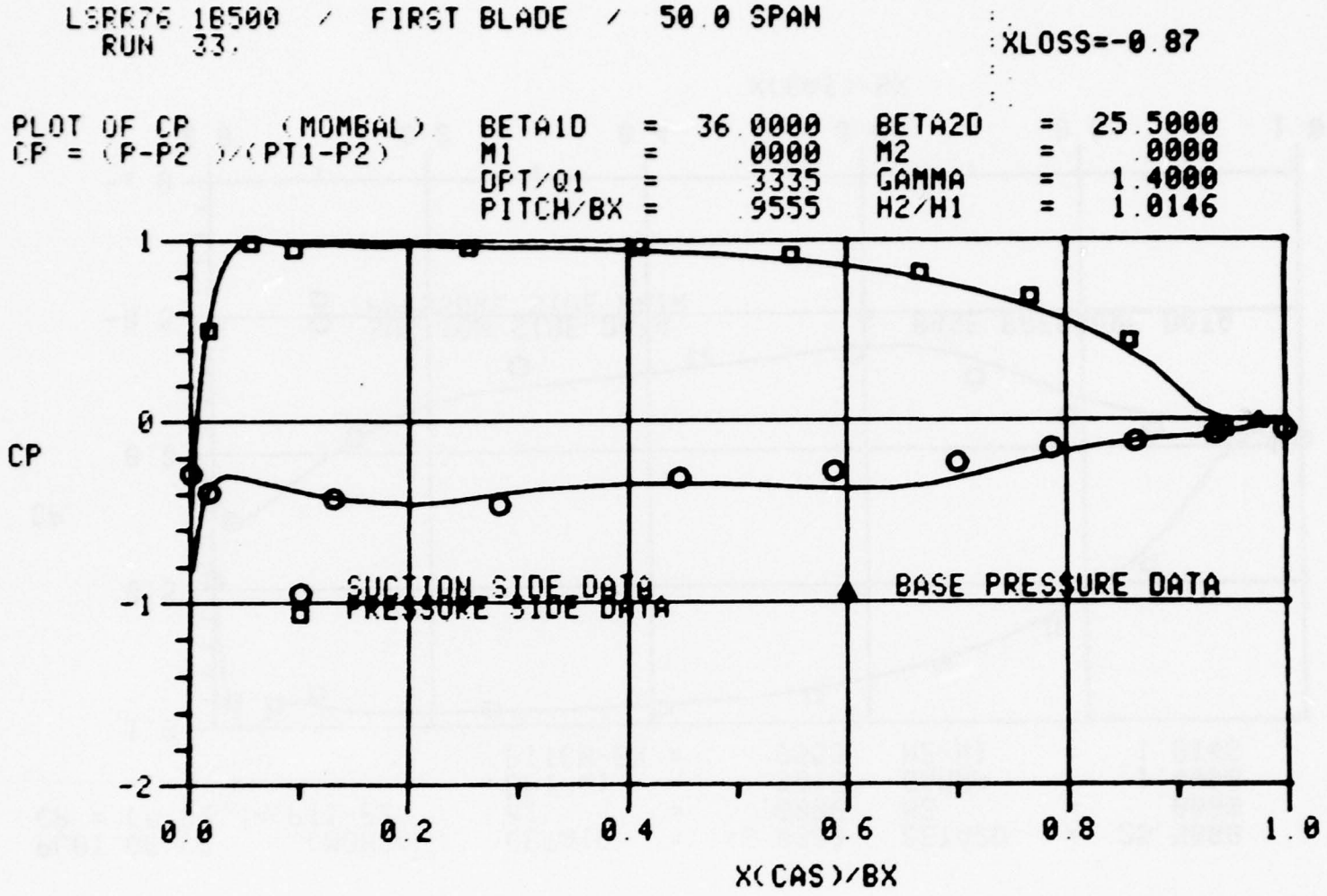

Figure 5. Rotor Midspan Pressure Distribution, $(C_x/U_m) = 0.955$

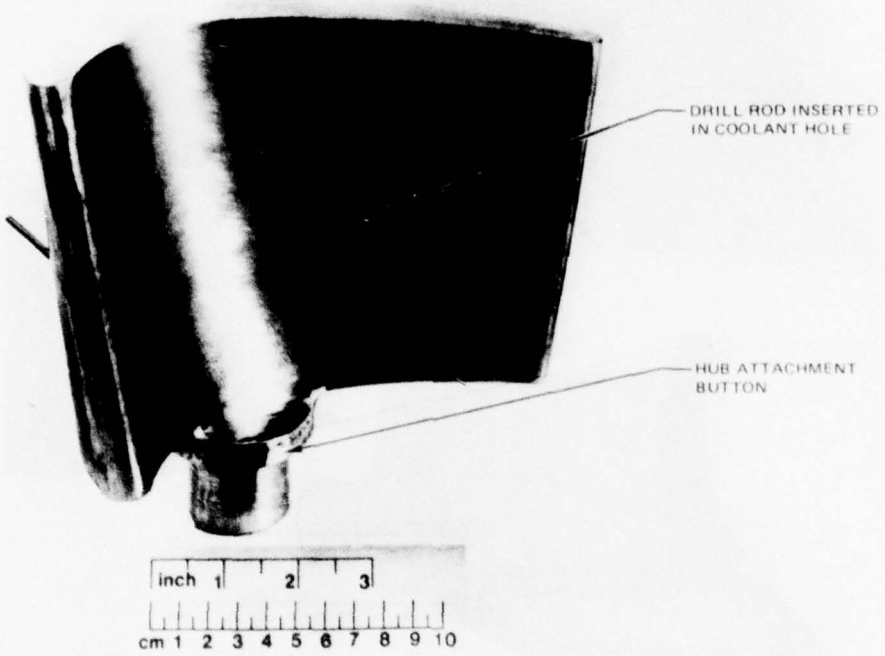

Figure 6. LSRR Turbine Rotor Master Metal Airfoil

77-308-F

77-08-295-1

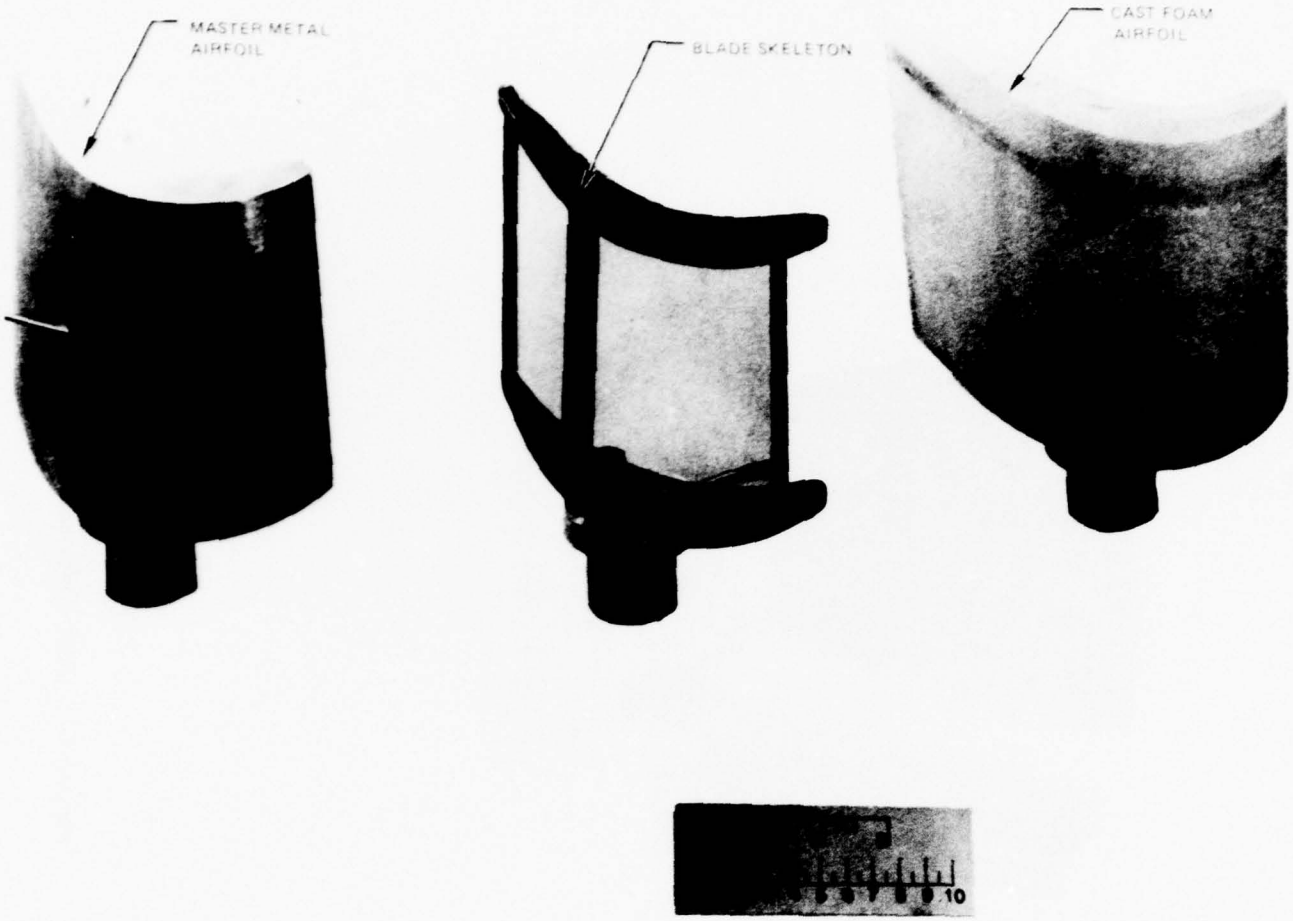

Figure 7. Foam Airfoil Model Fabrication Phases

Figure 8. Cast Foam Airfoil Model

77-308-G

77-08-295-3

Figure 9. Flow Visualization Test Points

78-02-208-4

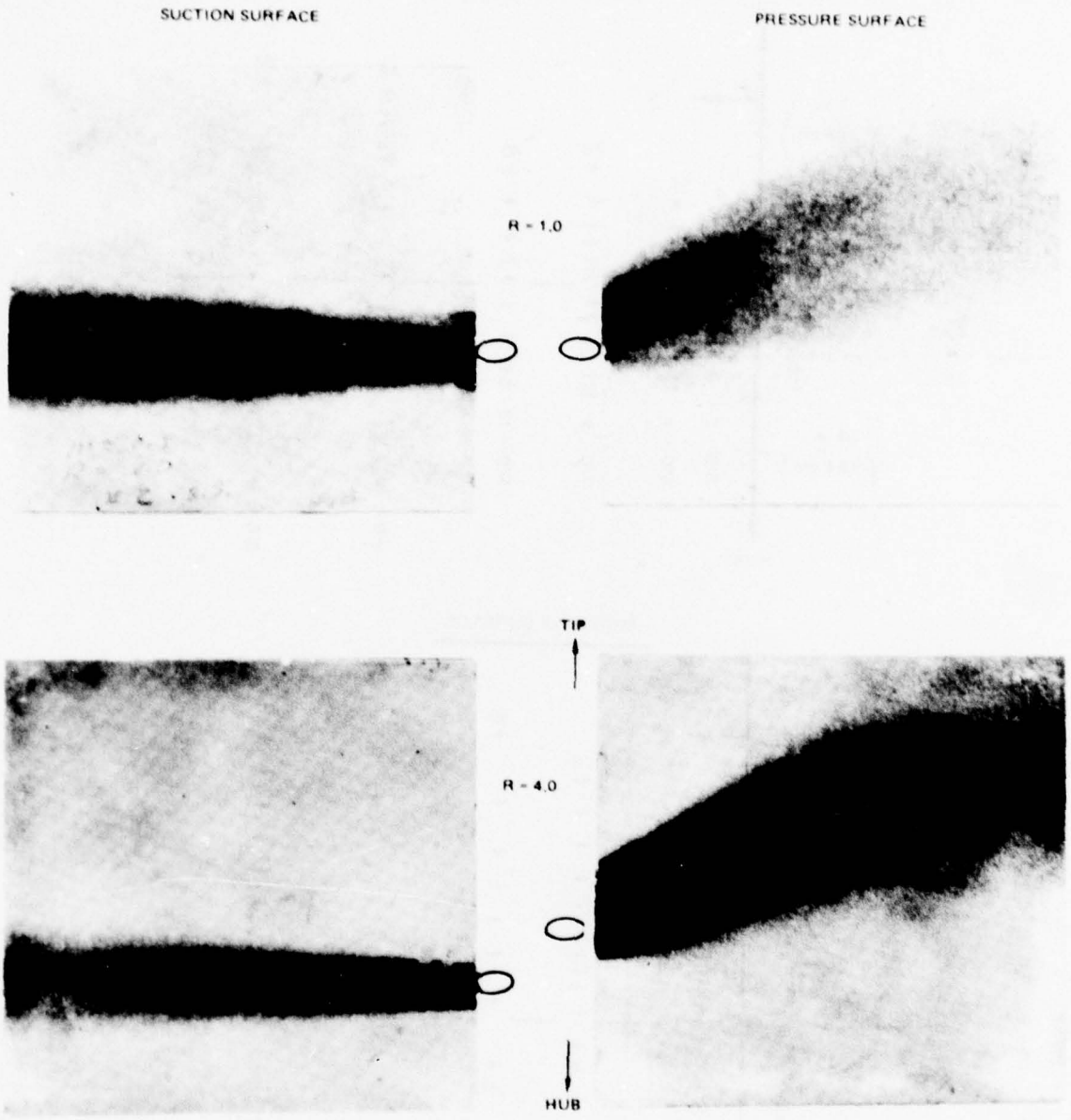

Figure 10. Film Coolant Trajectories at M≈0.5

78-02-208-5

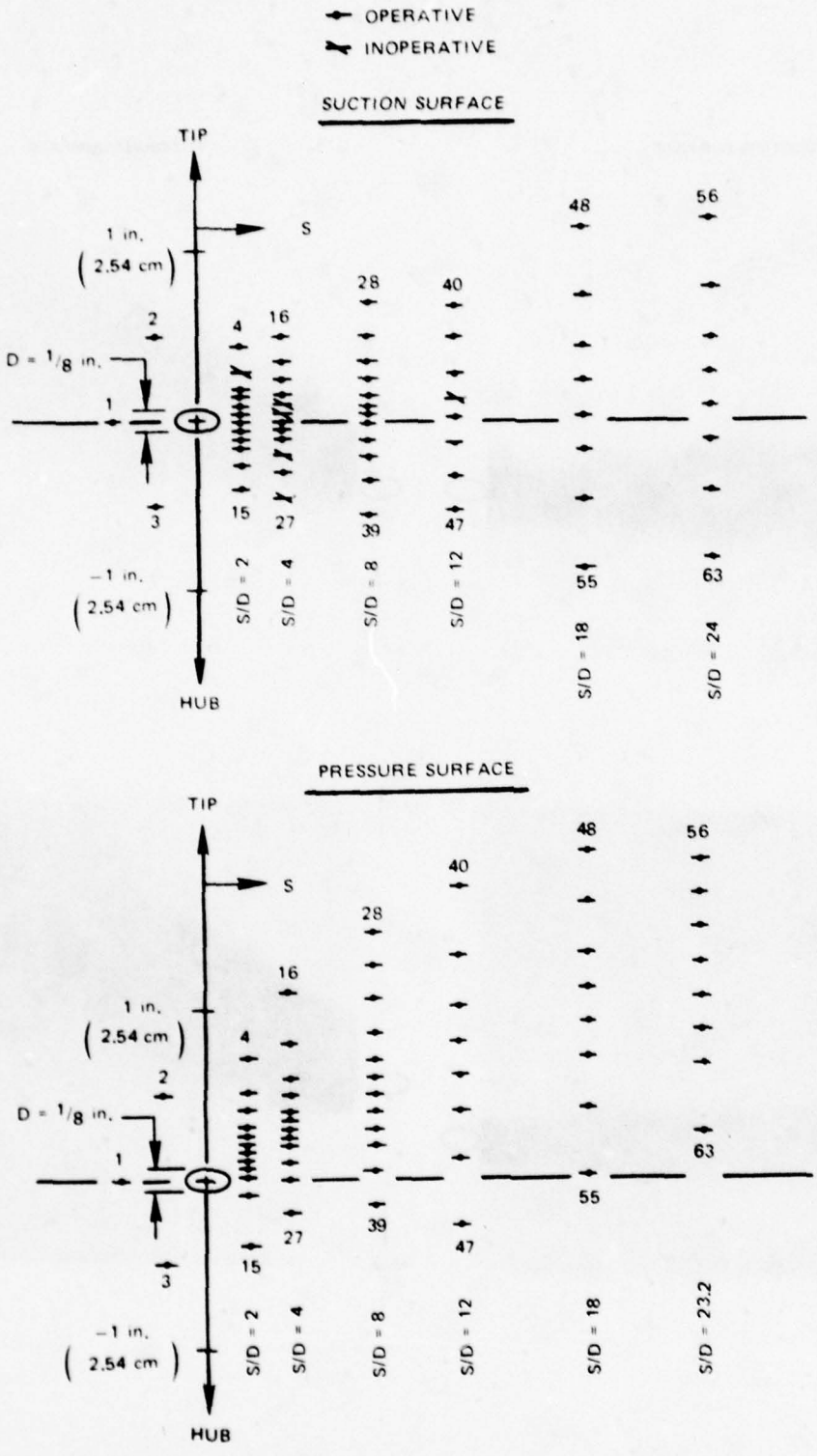

Figure 11. Thermocouple Arrays

78-06-97-1

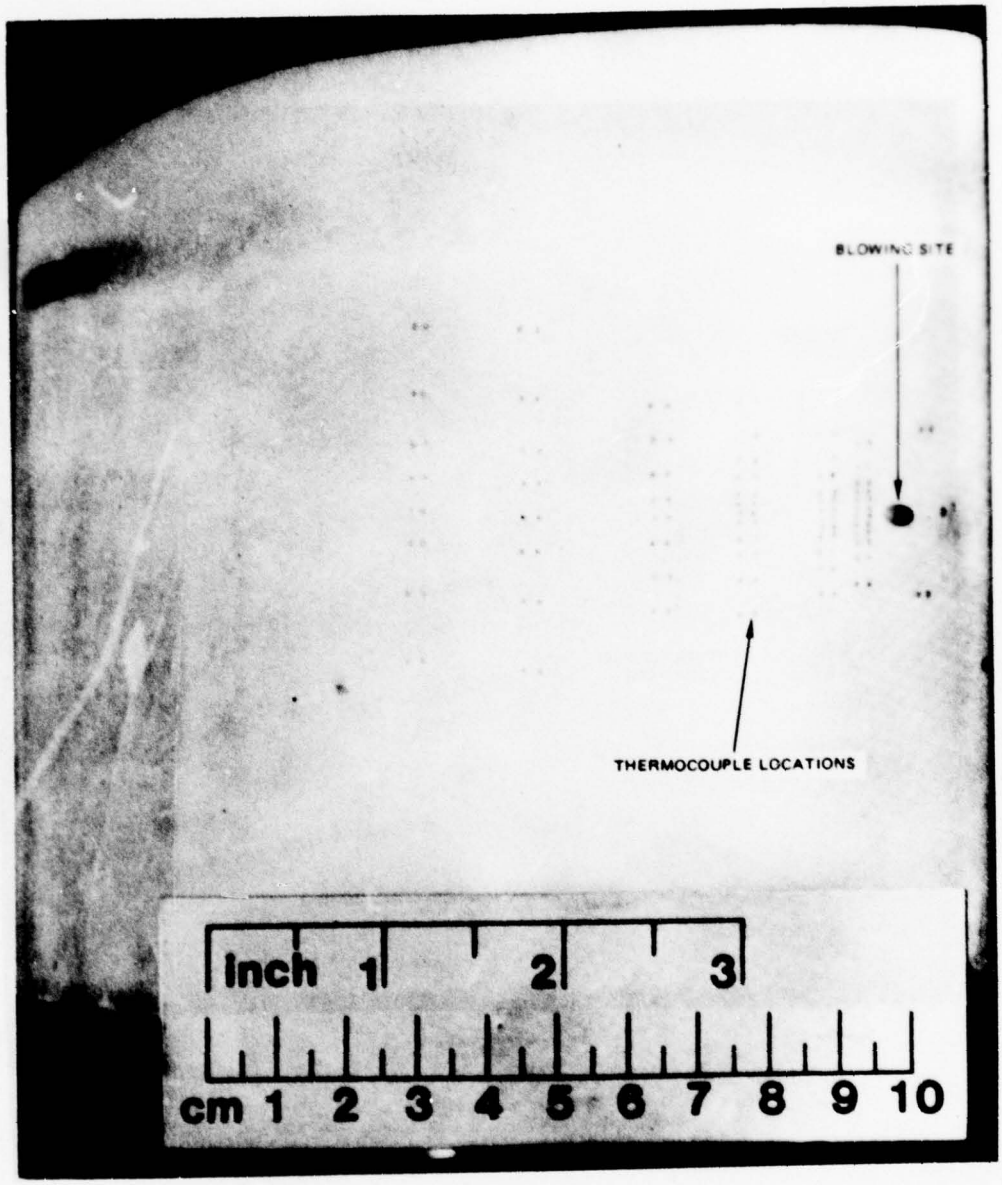

Figure 12. Thermocouple Array Locations On The Suction Surface

78-02-208-6

M = 1.5

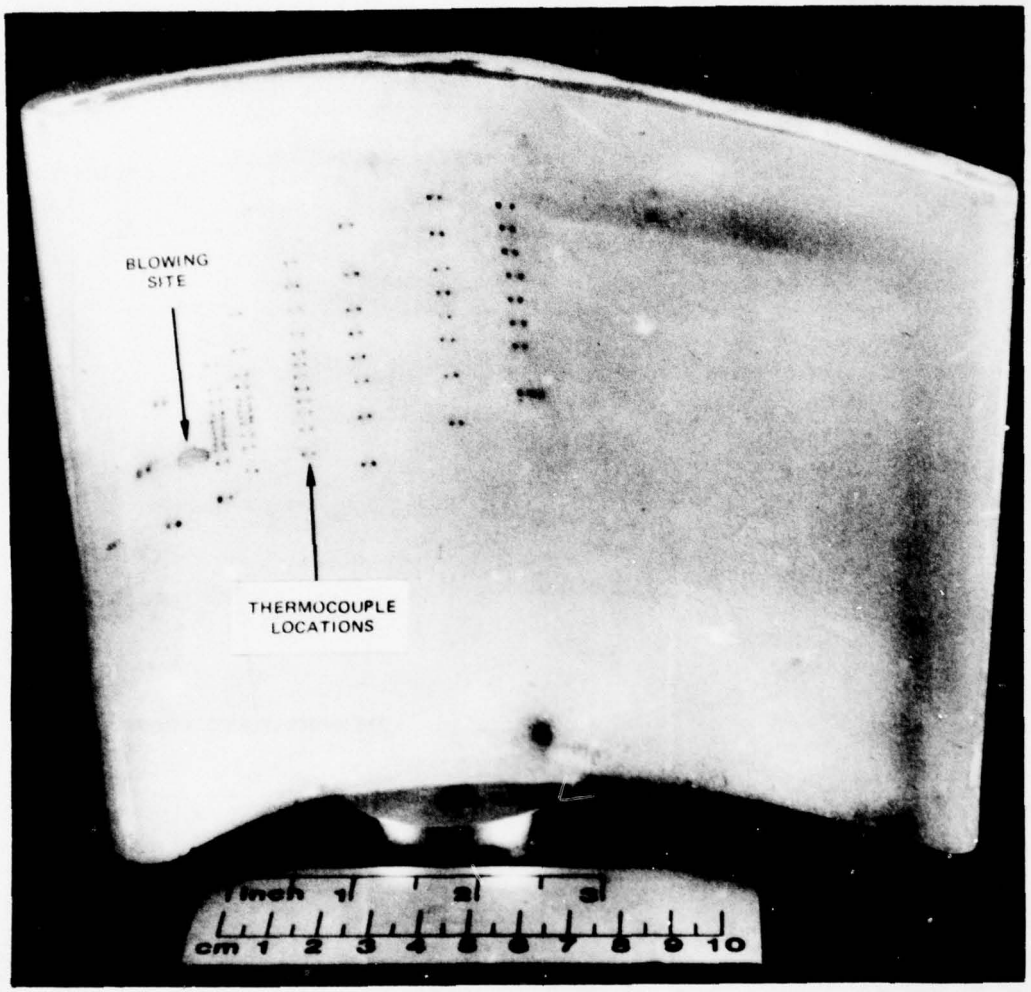

Figure 13. Thermocouple Array Locations On The Pressure Surface

78-141-A

78-06-141-1

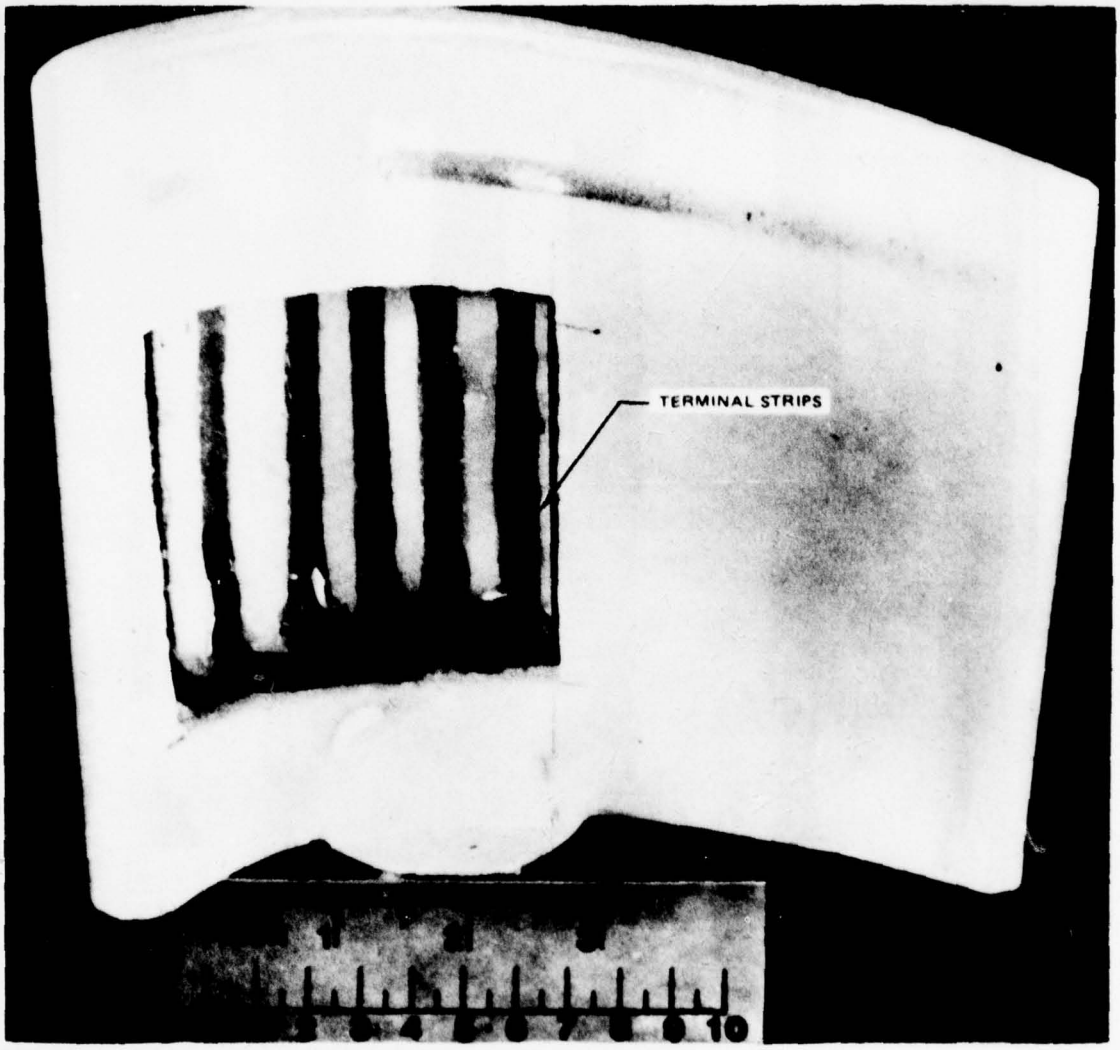

Figure 14. Thermocouple Terminal Strips For The Suction Surface Blowing Site

78-02-208-7

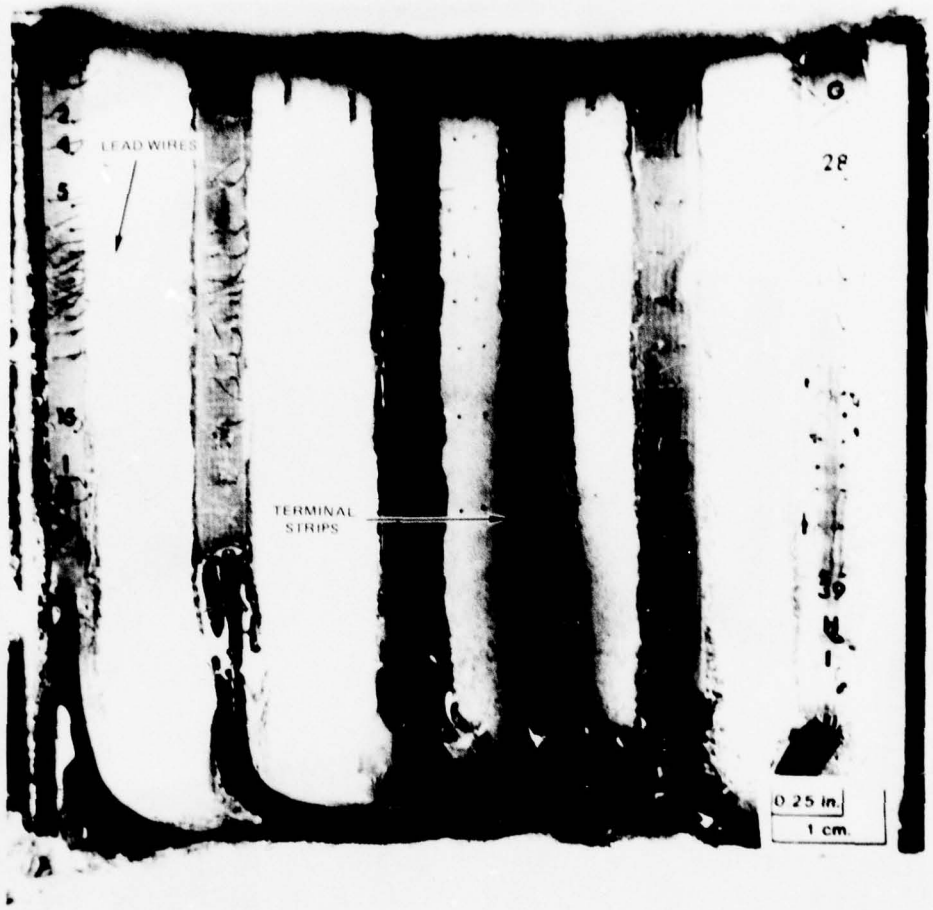

Figure 15. Terminal Strips And Lead Wires For The Suction Surface Blowing Site

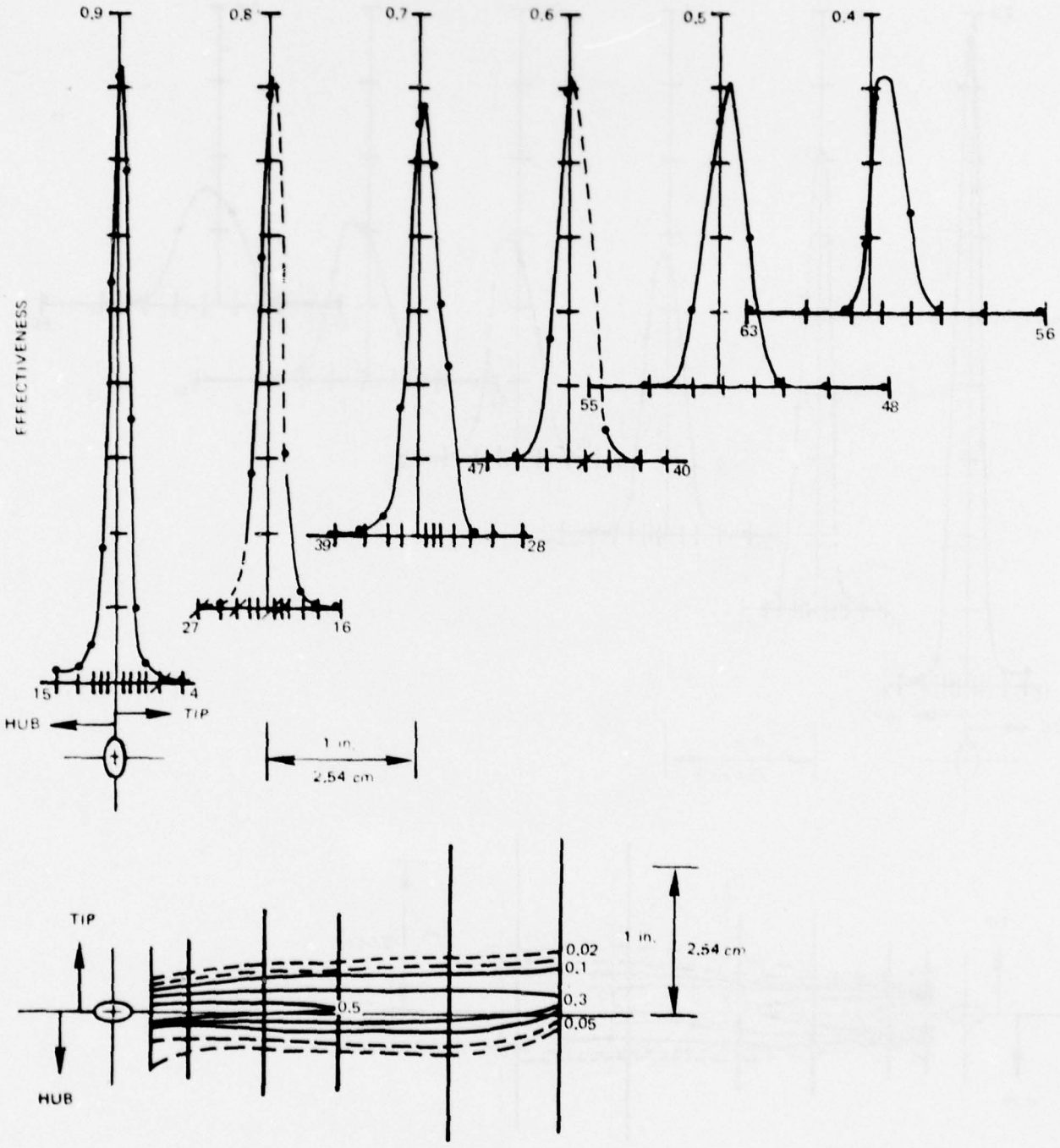

Figure 16. Suction Surface Film Cooling, M = 0.5, R = 1.0

78-06-157-8

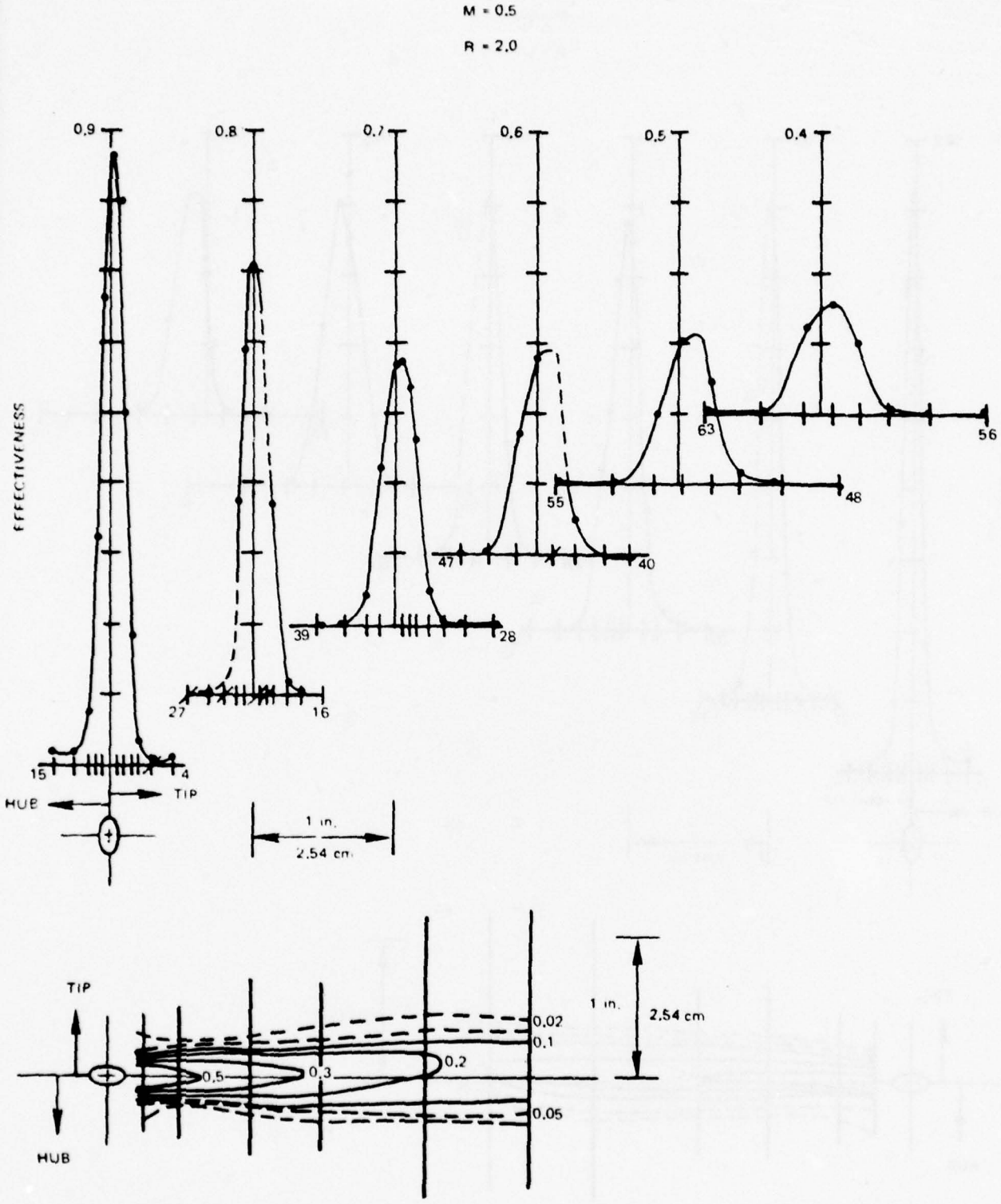

Figure 17. Suction Surface Film Cooling, M = 0.5, R = 2.0

78-06-157-10

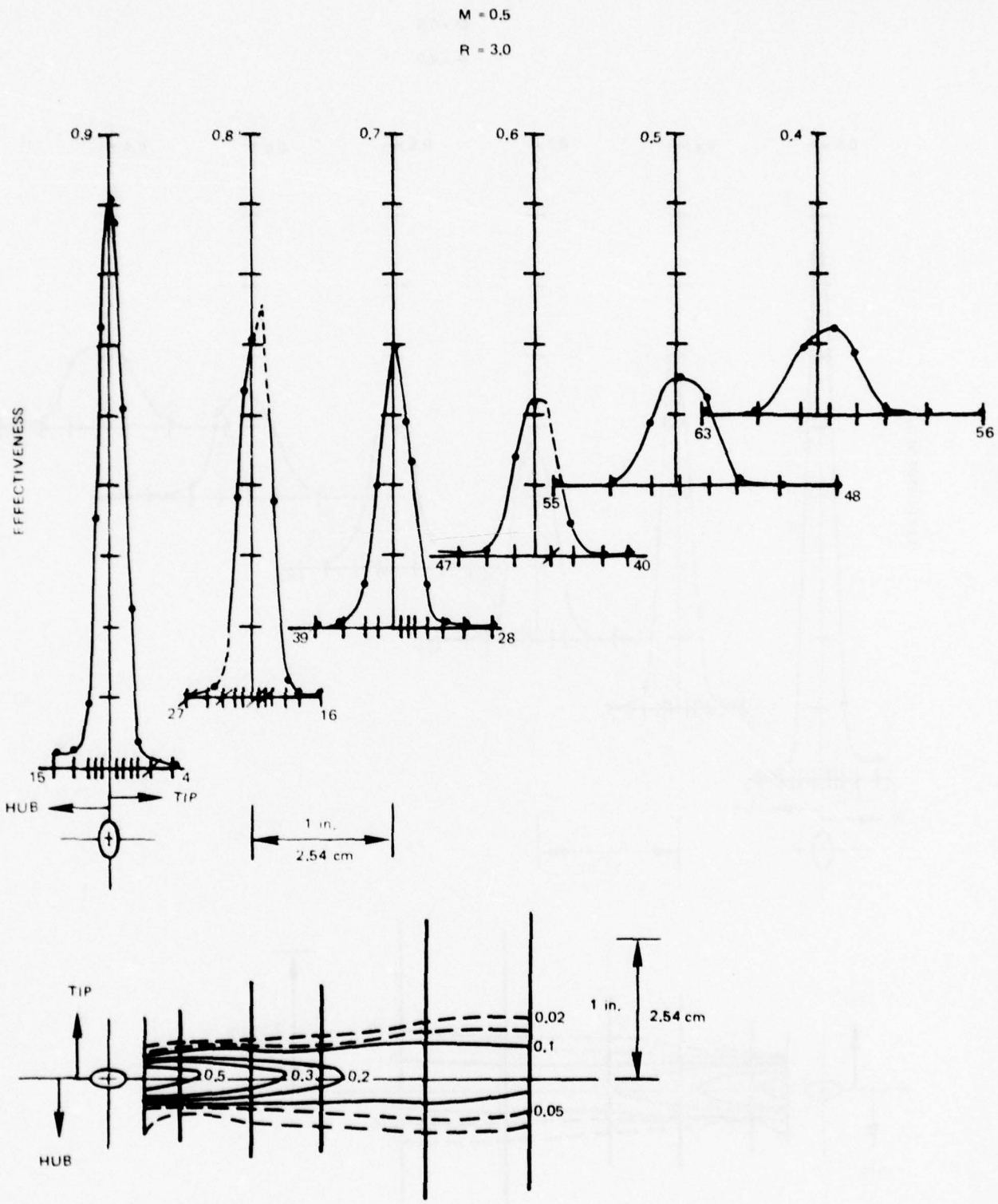

Figure 18. Suction Surface Film Cooling, M = 0.5, R = 3.0

78-06-157-9

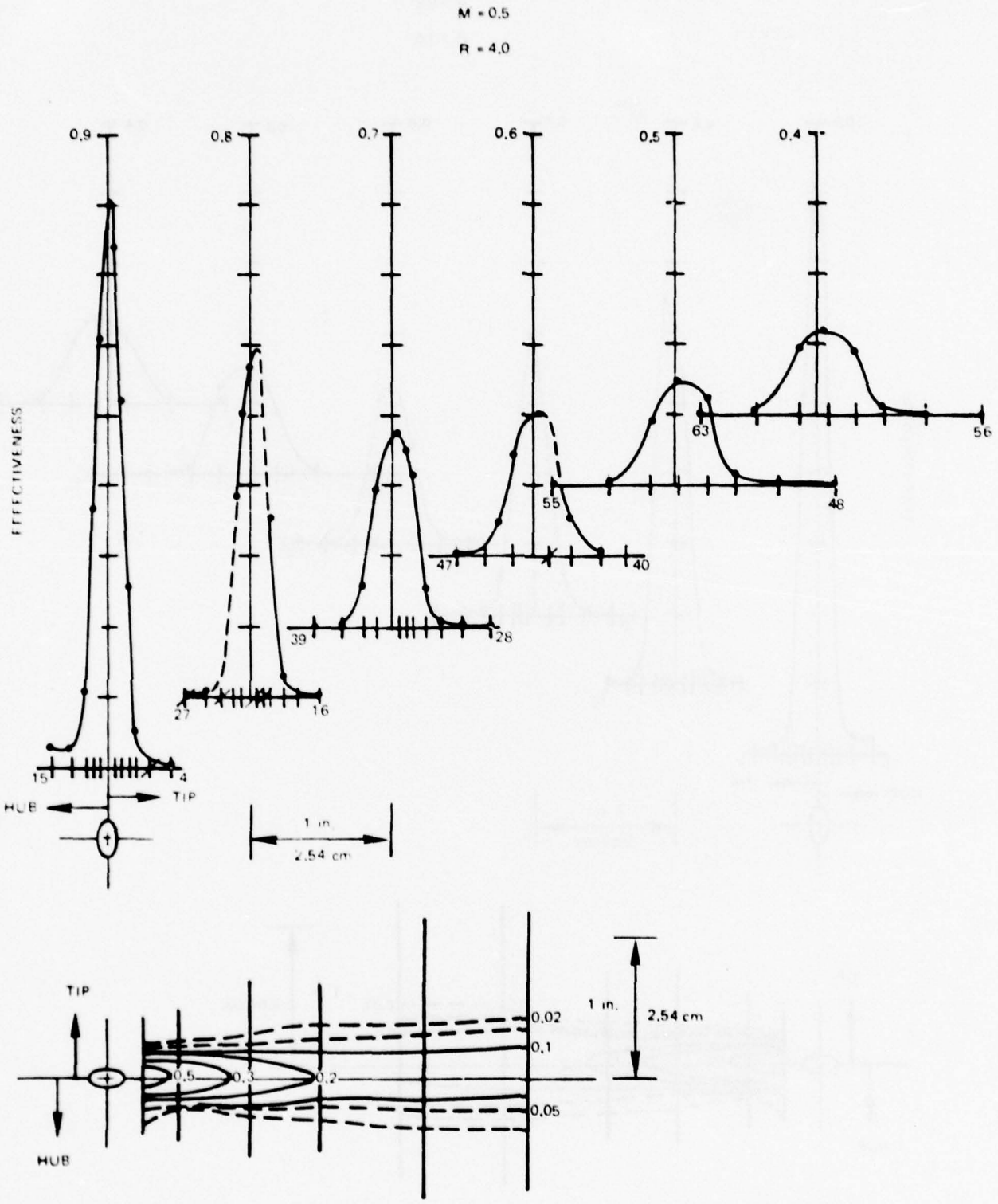

Figure 19. Suction Surface Film Cooling, M = 0.5, R = 4.0

78-06-157-11

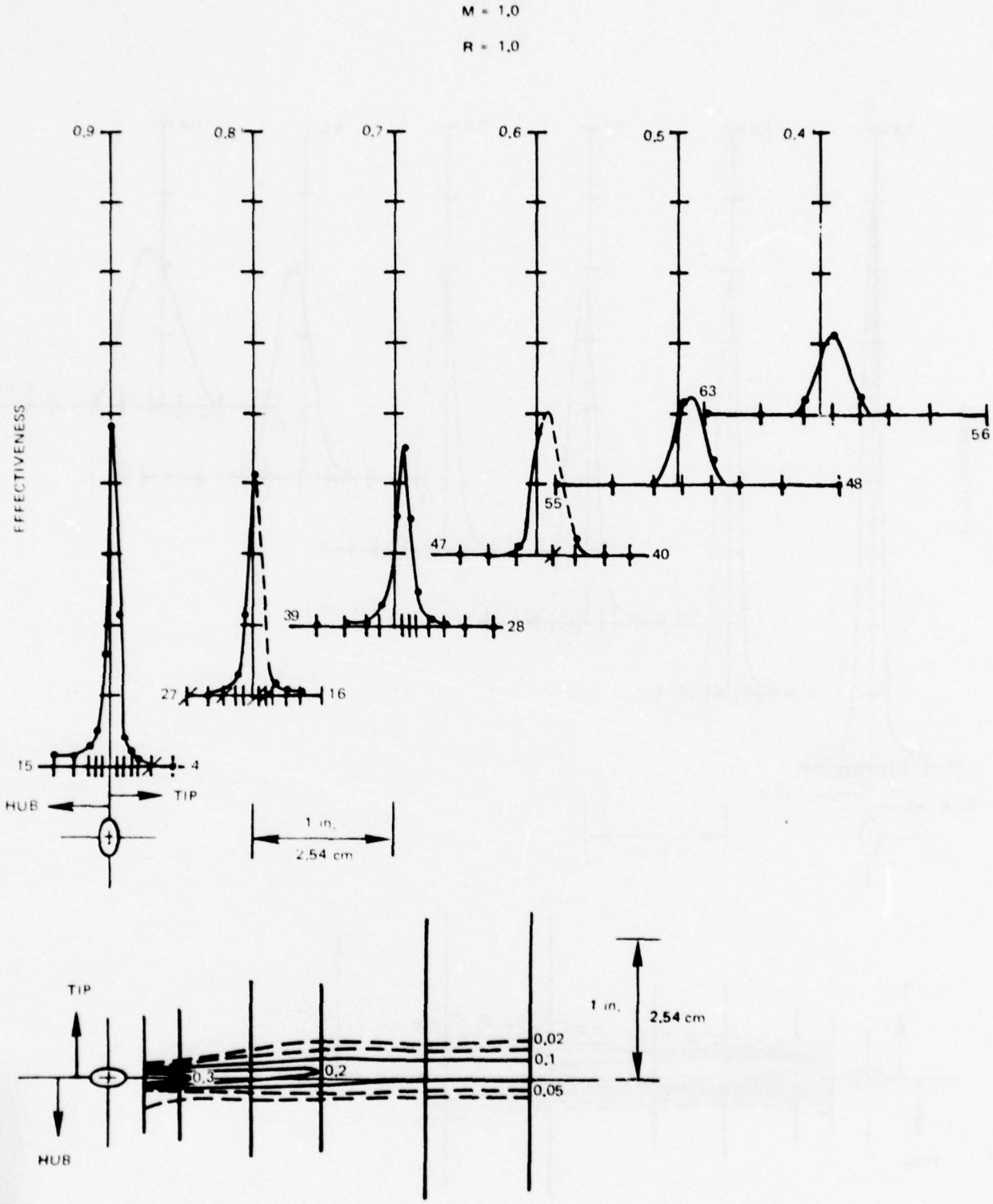

Figure 20. Suction Surface Film Cooling, M = 1.0, R = 1.0

78-06-157-3

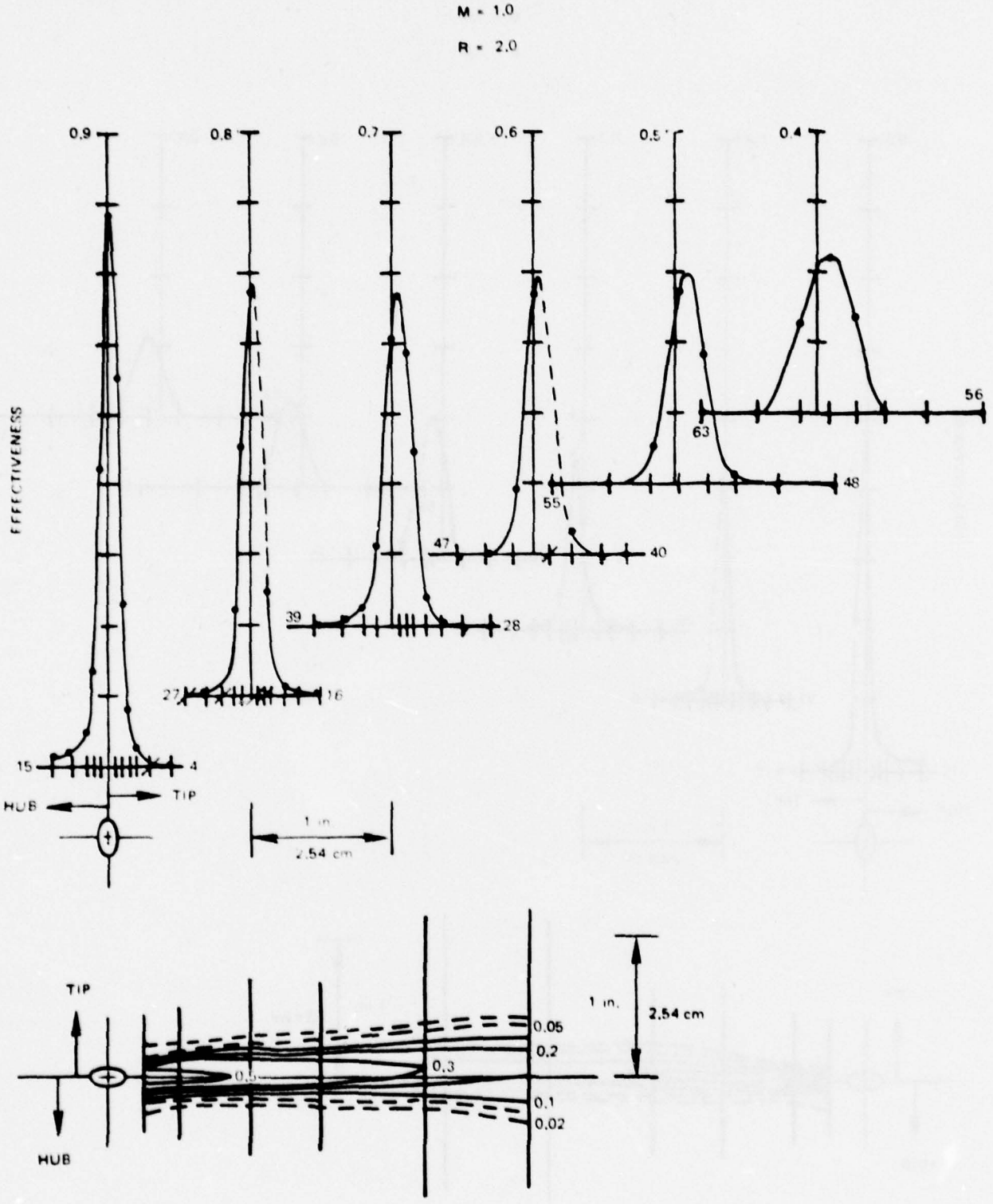

Figure 21. Suction Surface Film Cooling, M = 1.0, R = 2.0

78-06-157-6

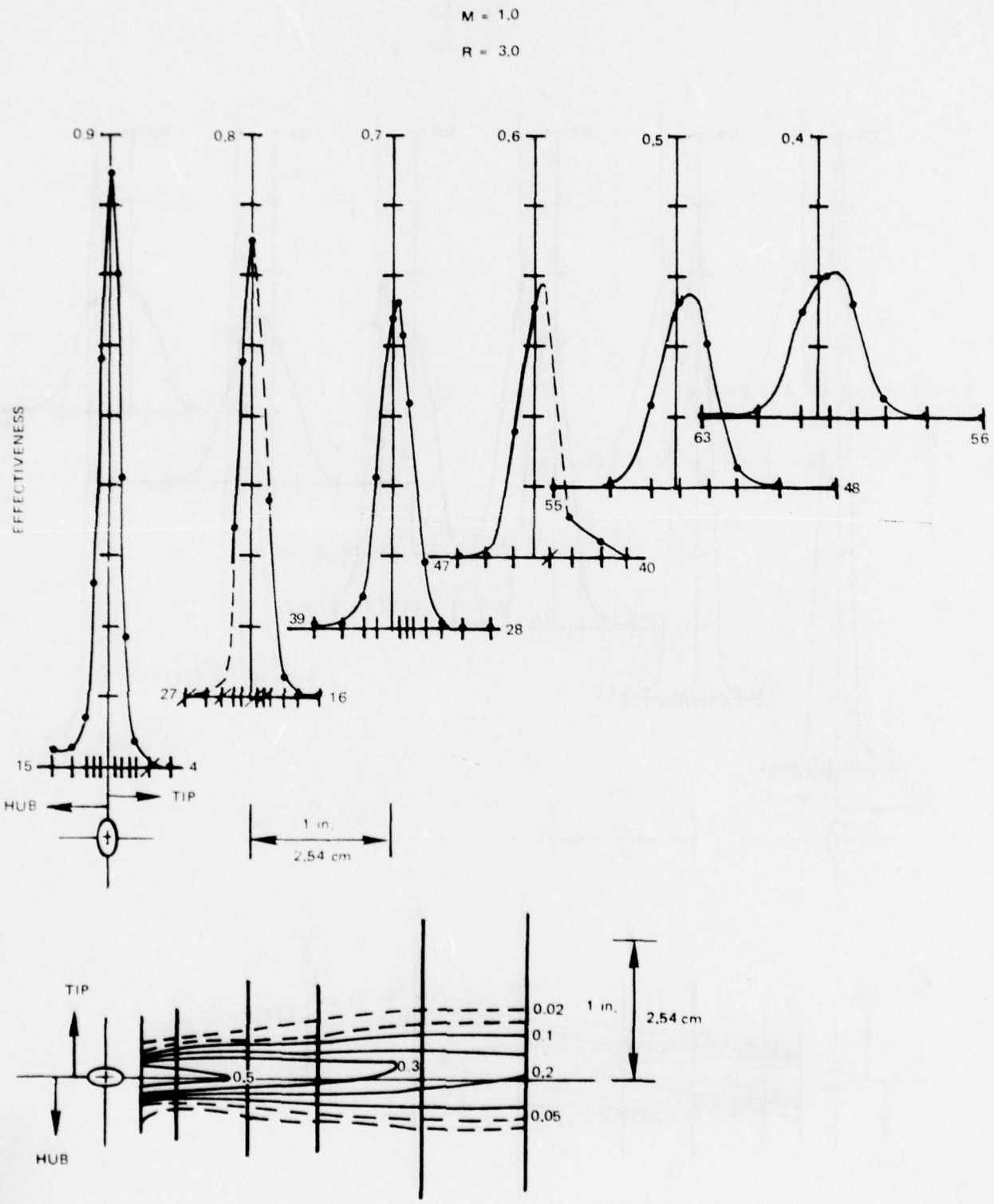

Figure 22. Suction Surface Film Cooling, M = 1.0, R = 3.0

78-06-157-5

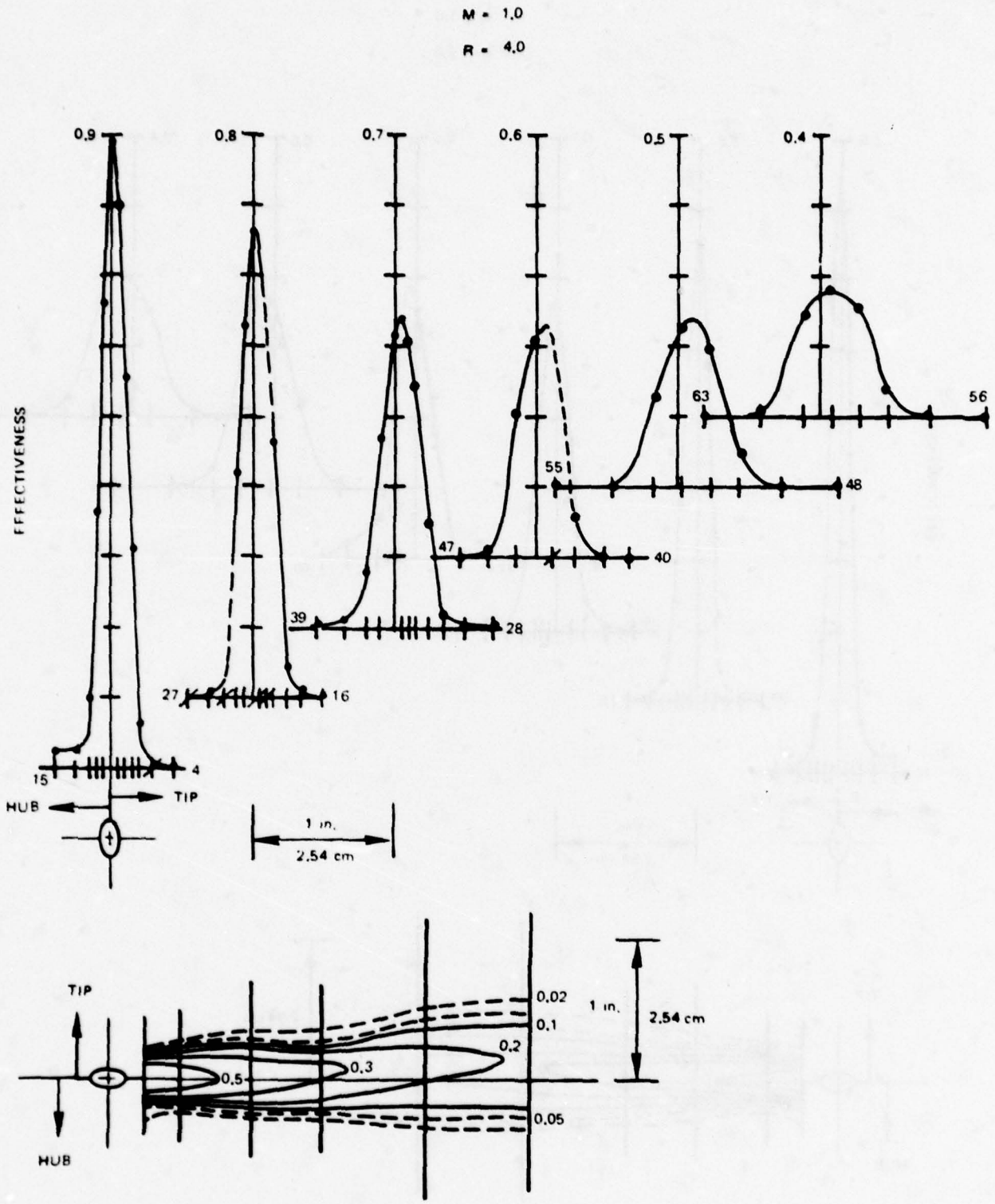

Figure 23. Suction Surface Film Cooling, M = 1.0, R = 4.0

78-06-157-2

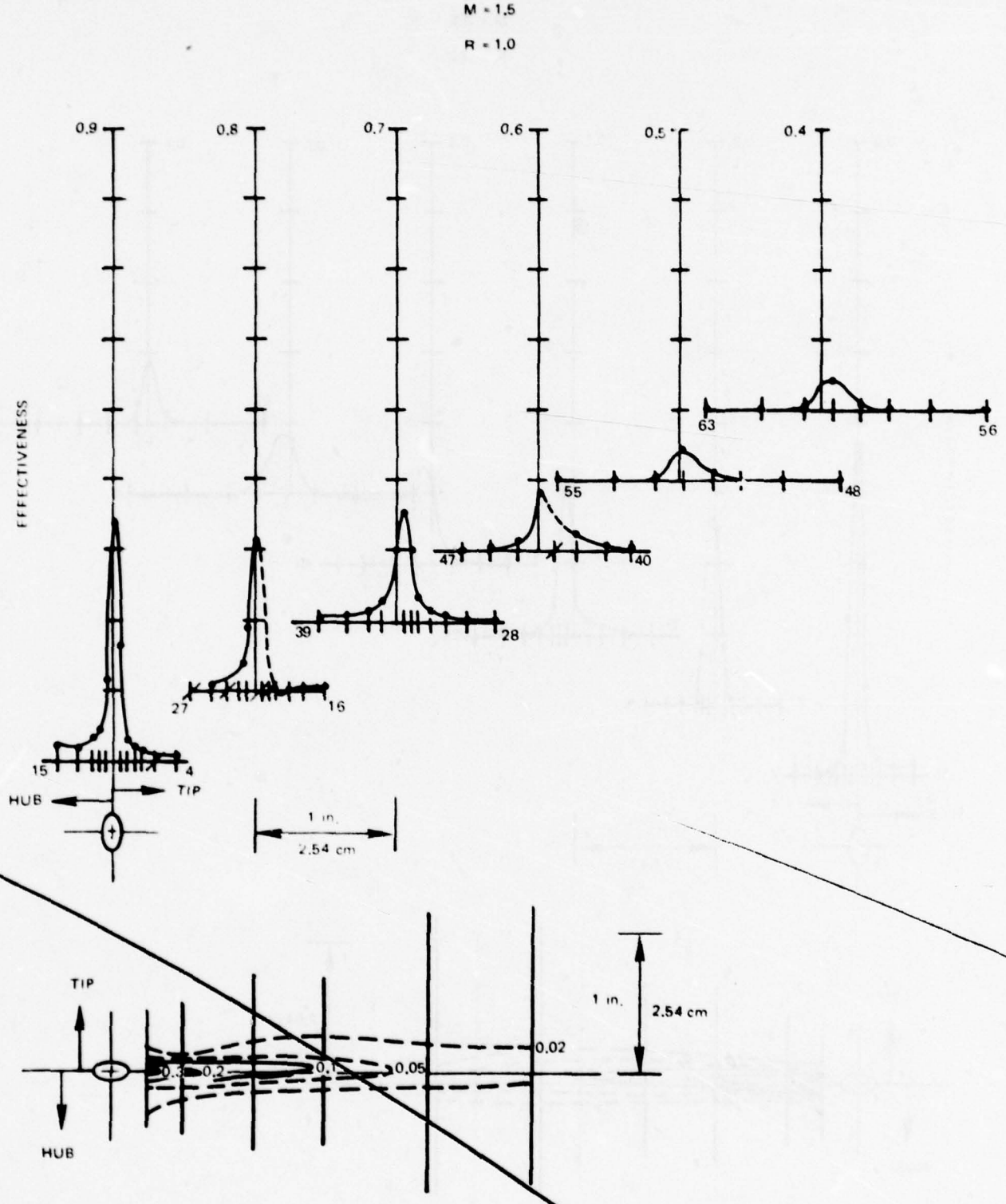

Figure 24. Suction Surface Film Cooling, M = 1.5, R = 1.0

78-06-157-12

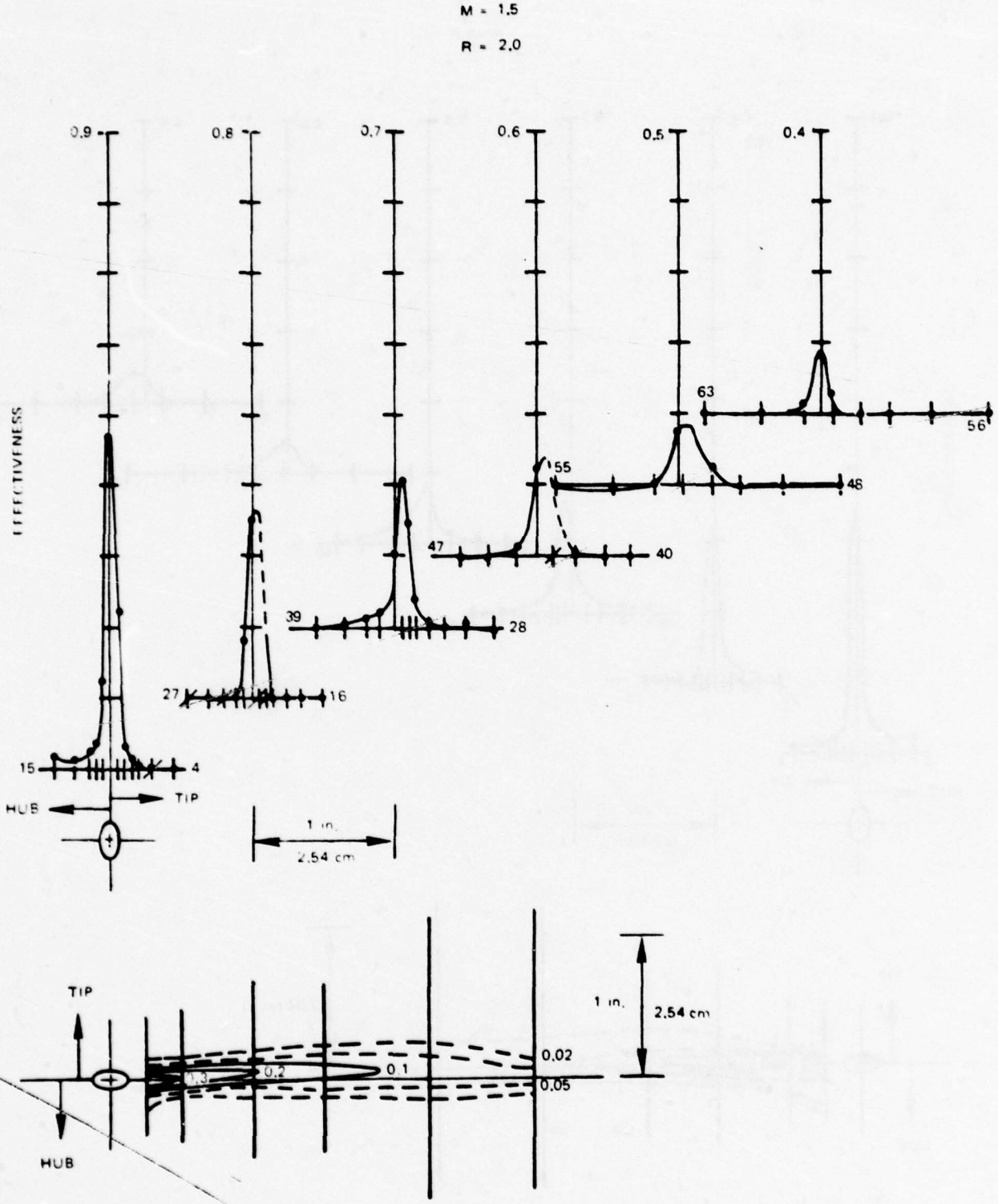

Figure 25. Suction Surface Film Cooling, M = 1.5, R = 2.0

78-06-157-7

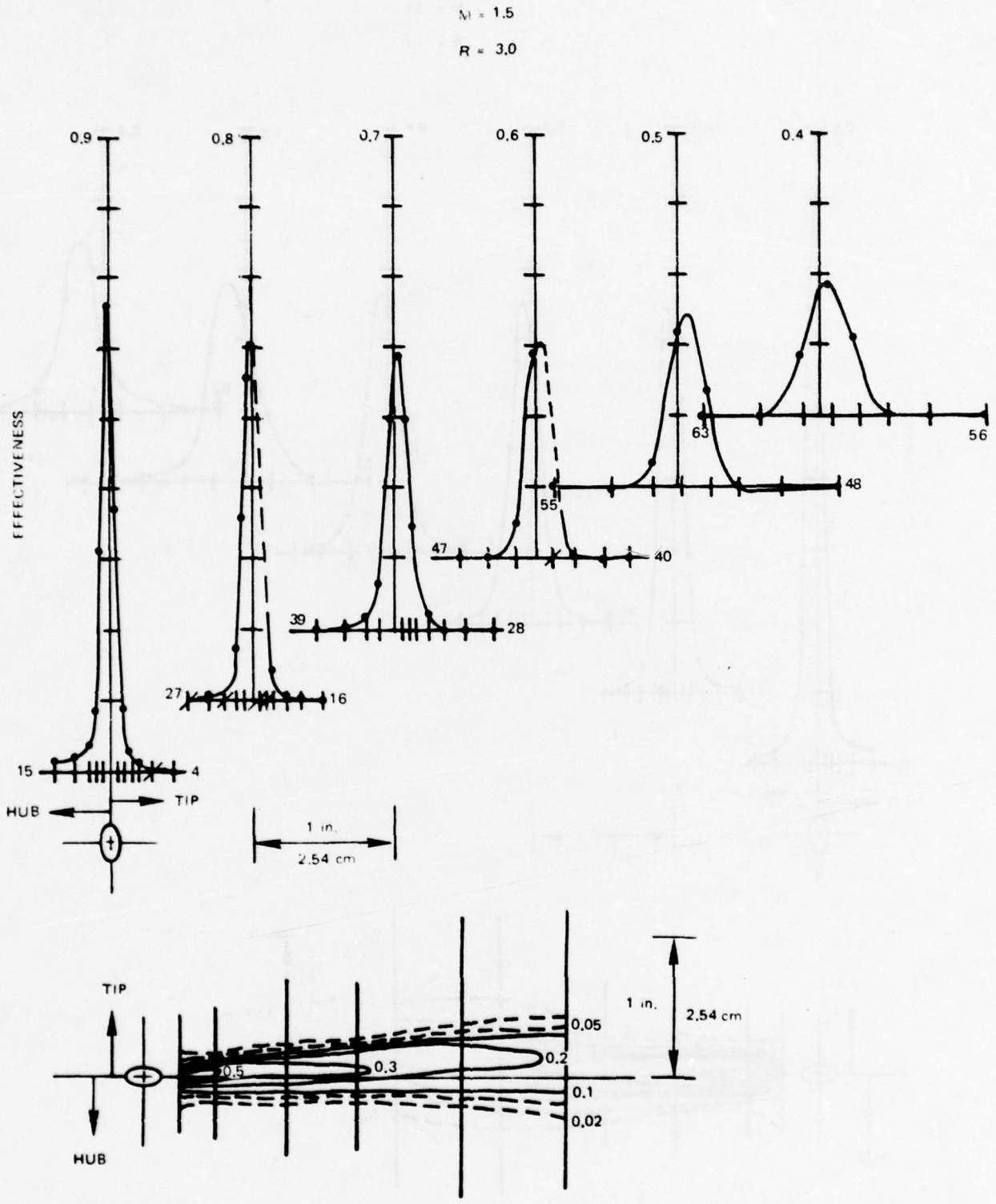

Figure 26. Suction Surface Film Cooling, M = 1.5, R = 3.0

78-06-157-4

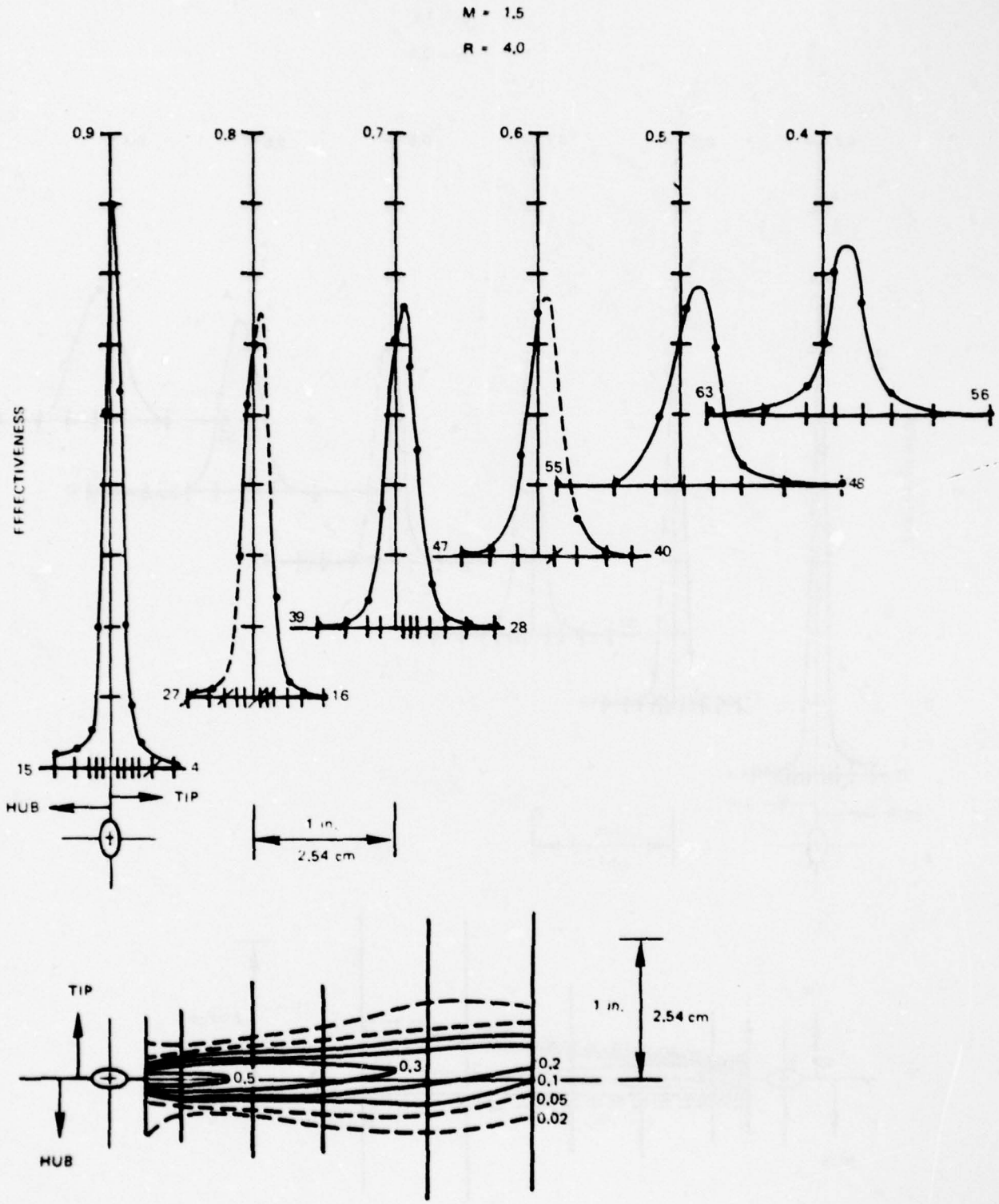

Figure 27. Suction Surface Film Cooling, M = 1.5, R = 4.0

78-06-157-1

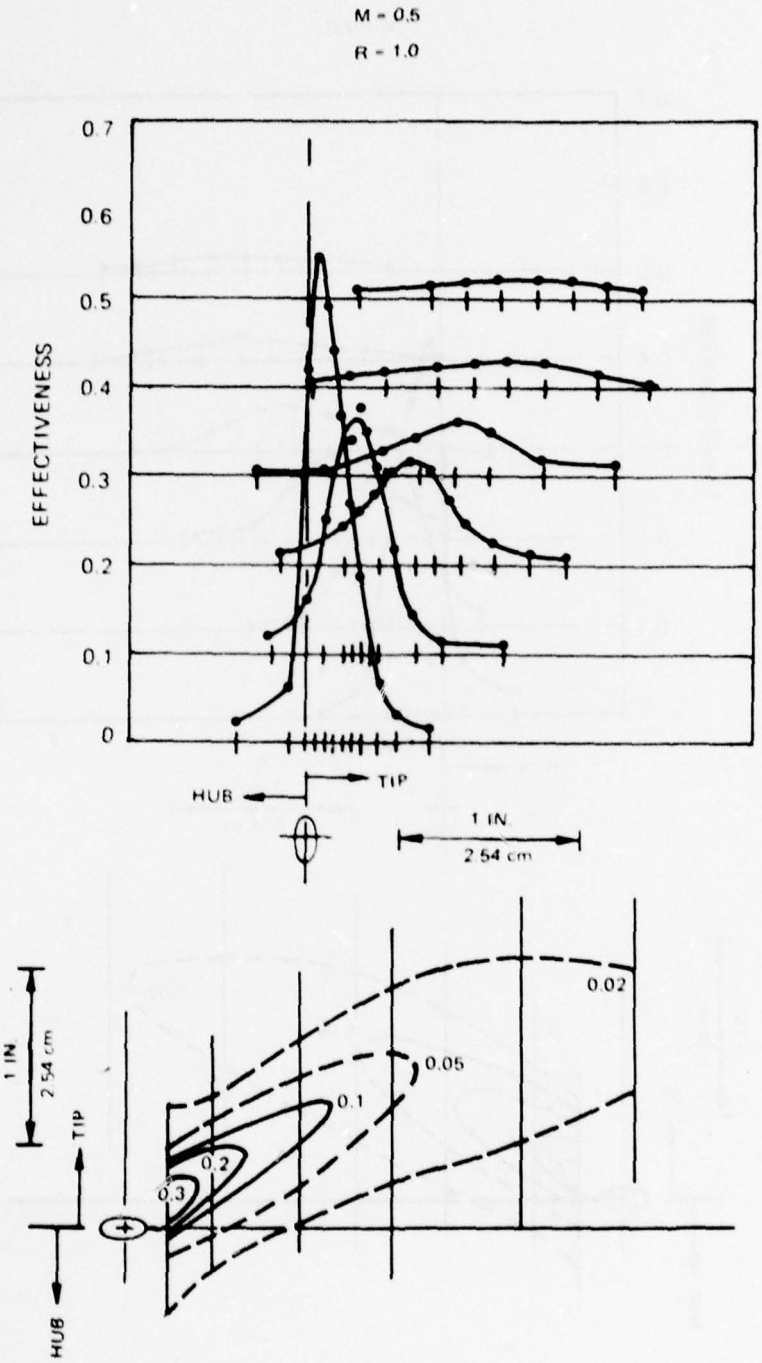

Figure 28. Pressure Surface Film Cooling, M = 0.5, R = 1.0

78-06-31-3

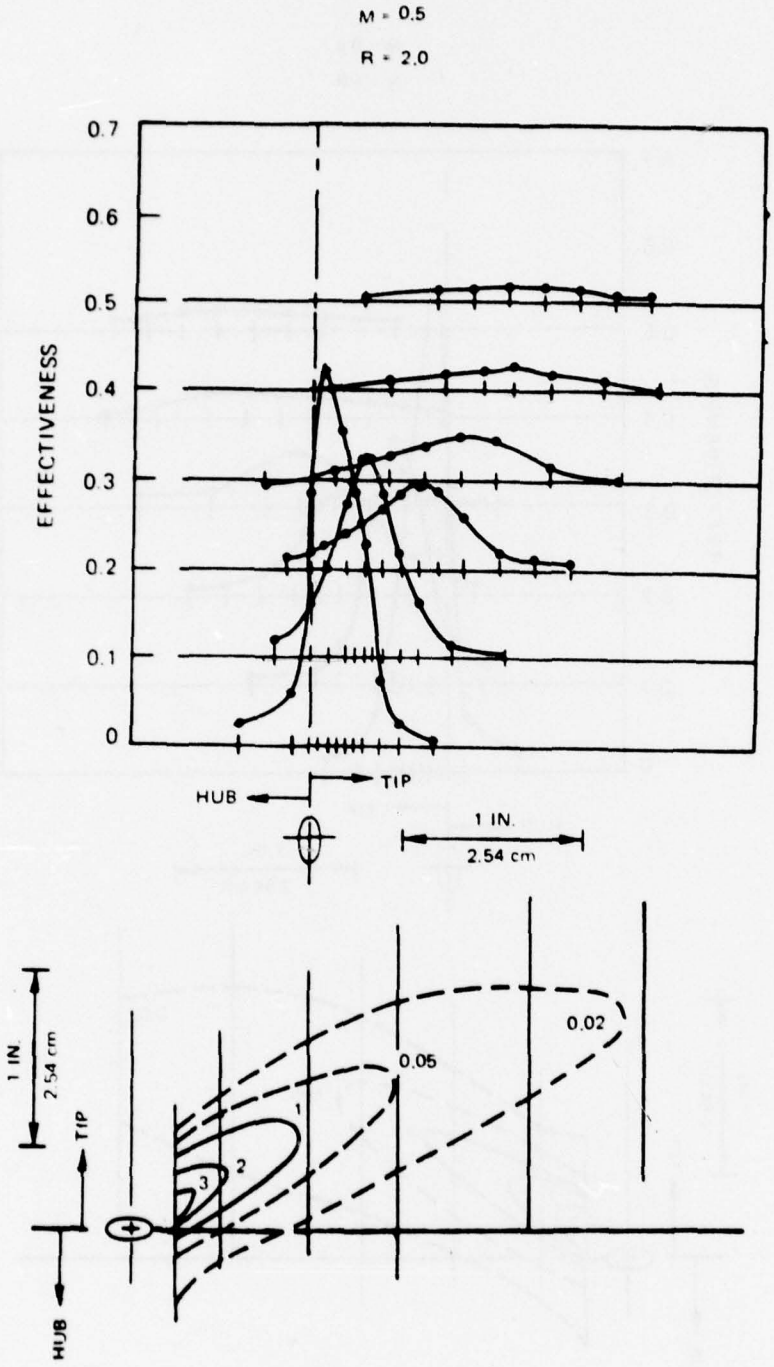

Figure 29. Pressure Surface Film Cooling, M = 0.5, R = 2.0

78-06-31-1

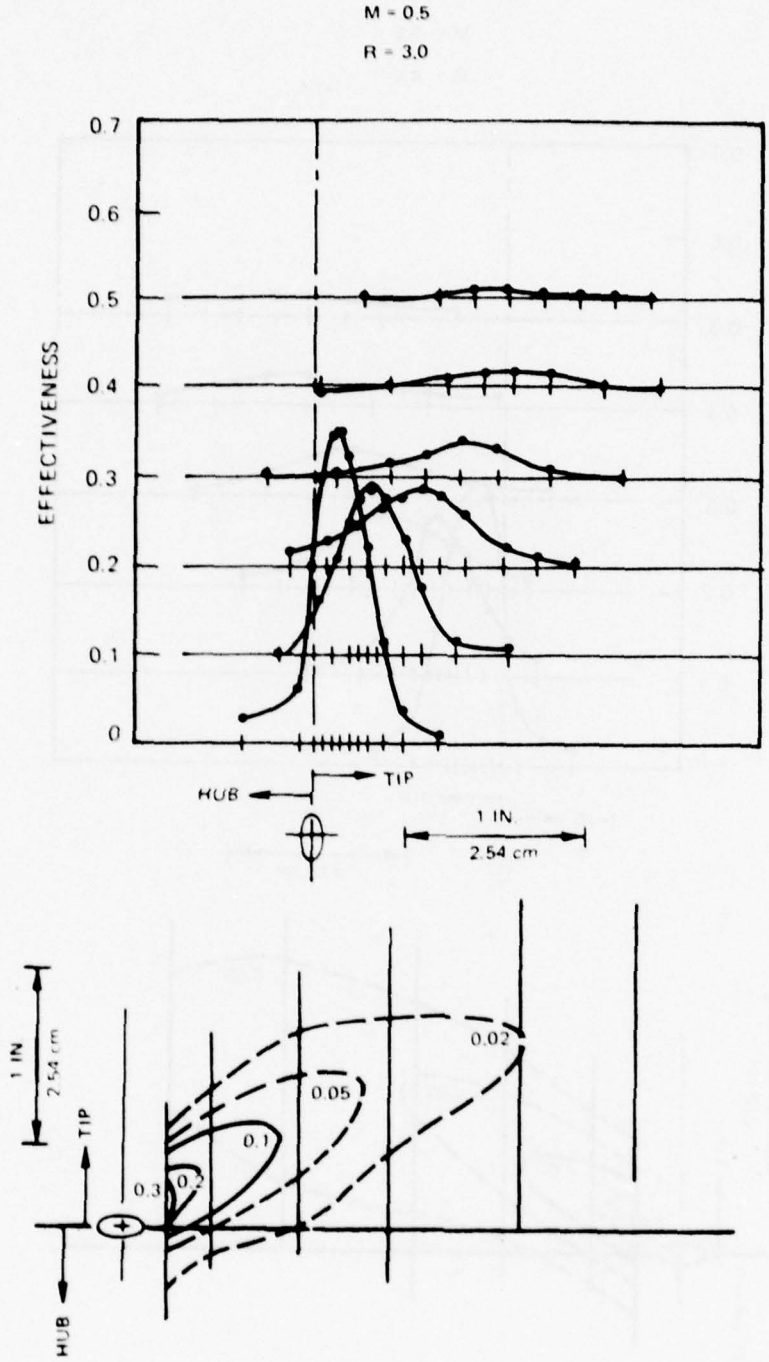

Figure 30. Pressure Surface Film Cooling, M = 0.5, R = 3.0

78-06-31-2

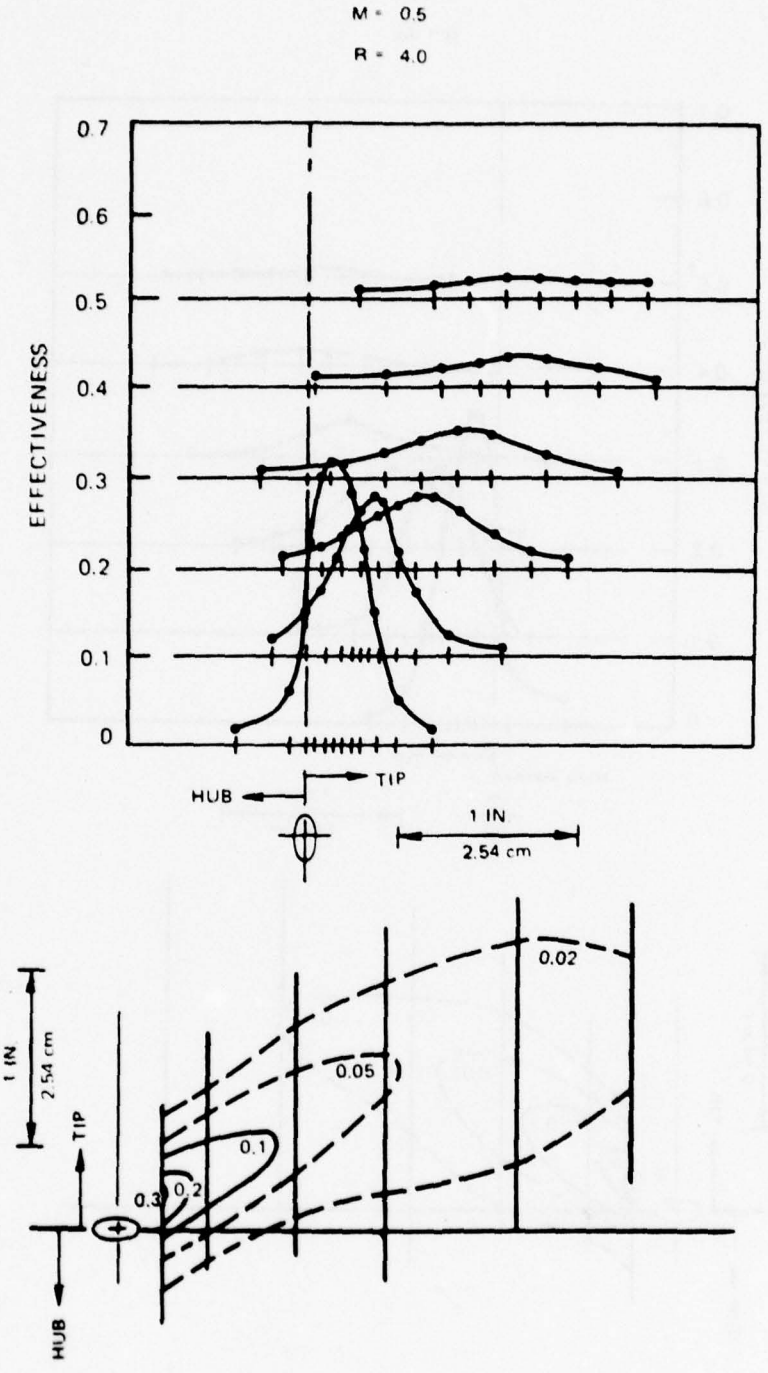

Figure 31. Pressure Surface Film Cooling, M = 0.5, R = 4.0

78-06-31-11

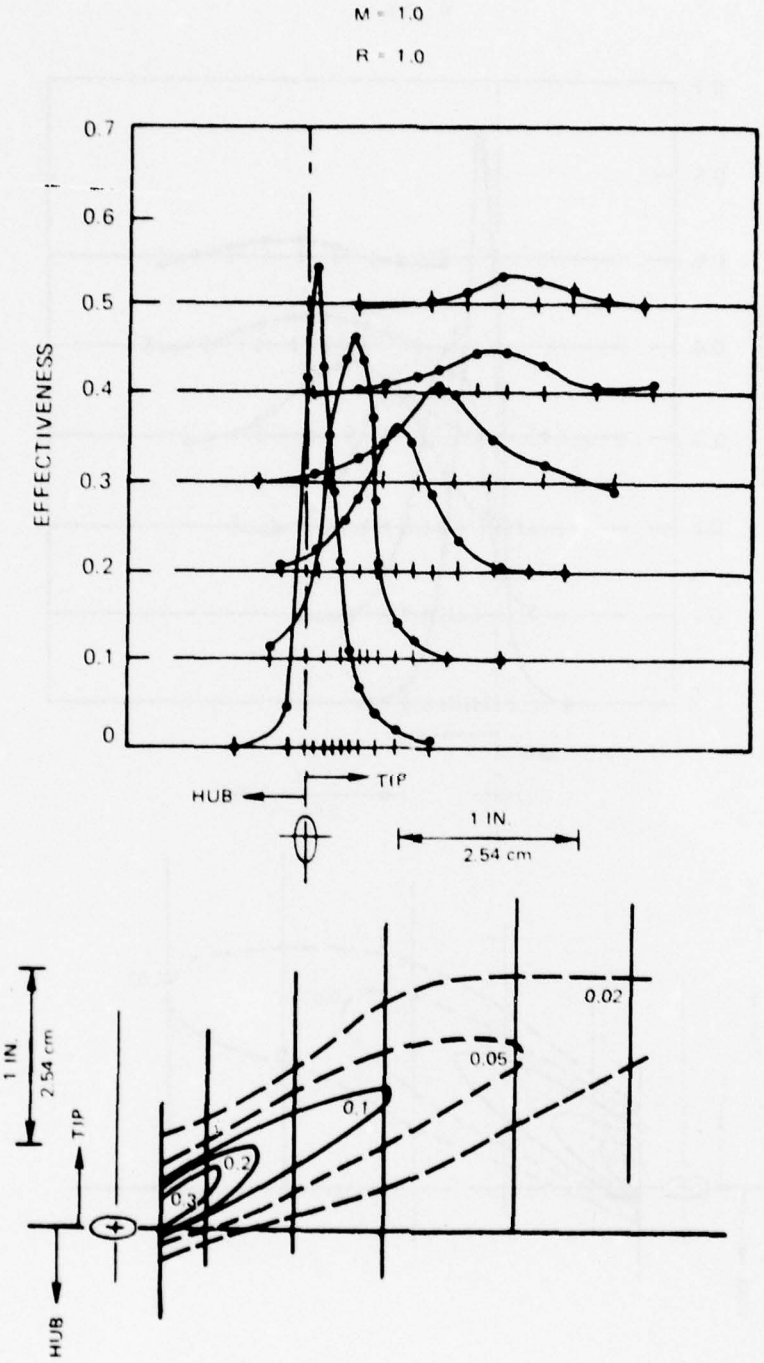

Figure 32. Pressure Surface Film Cooling, M = 1.0, R = 1.0

78-06-31-8

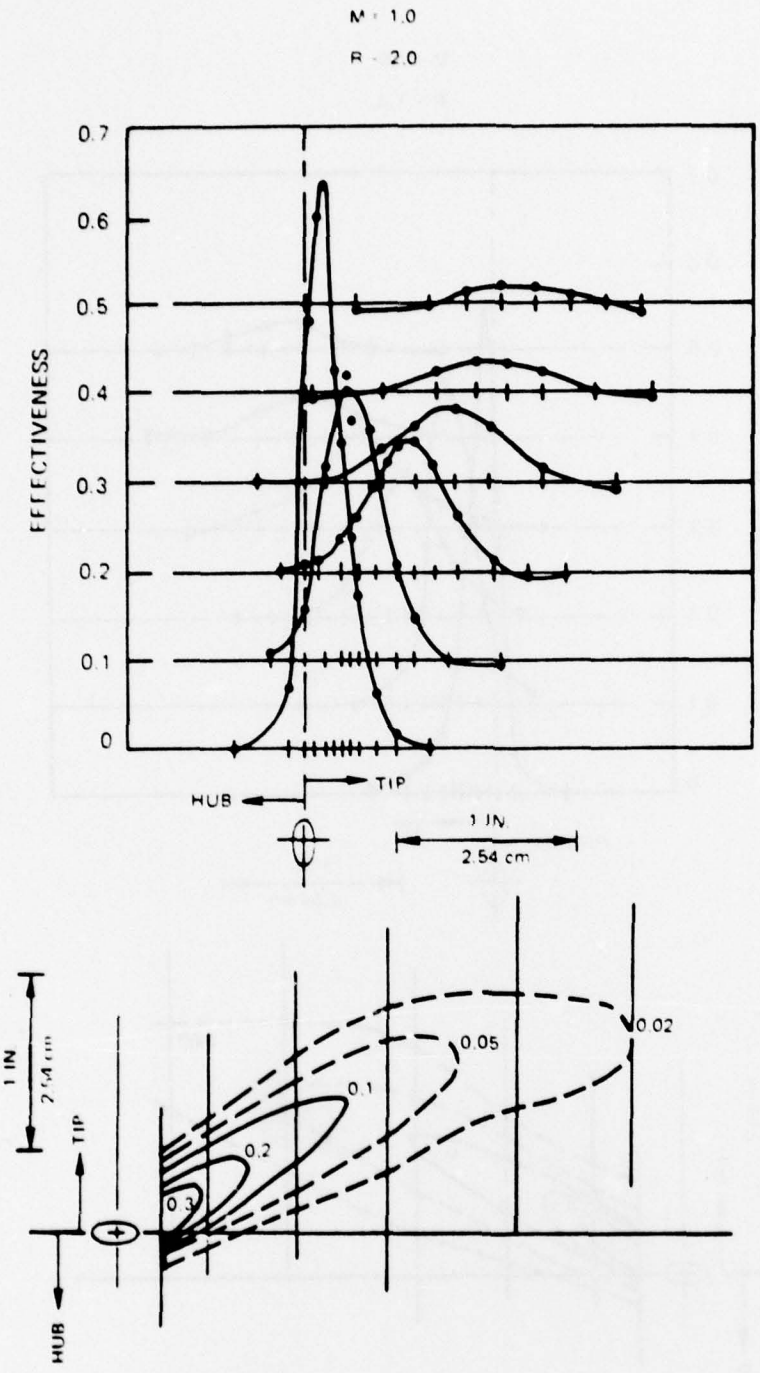

Figure 33. Pressure Surface Film Cooling, M = 1.0, R = 2.0

78-06-31-10

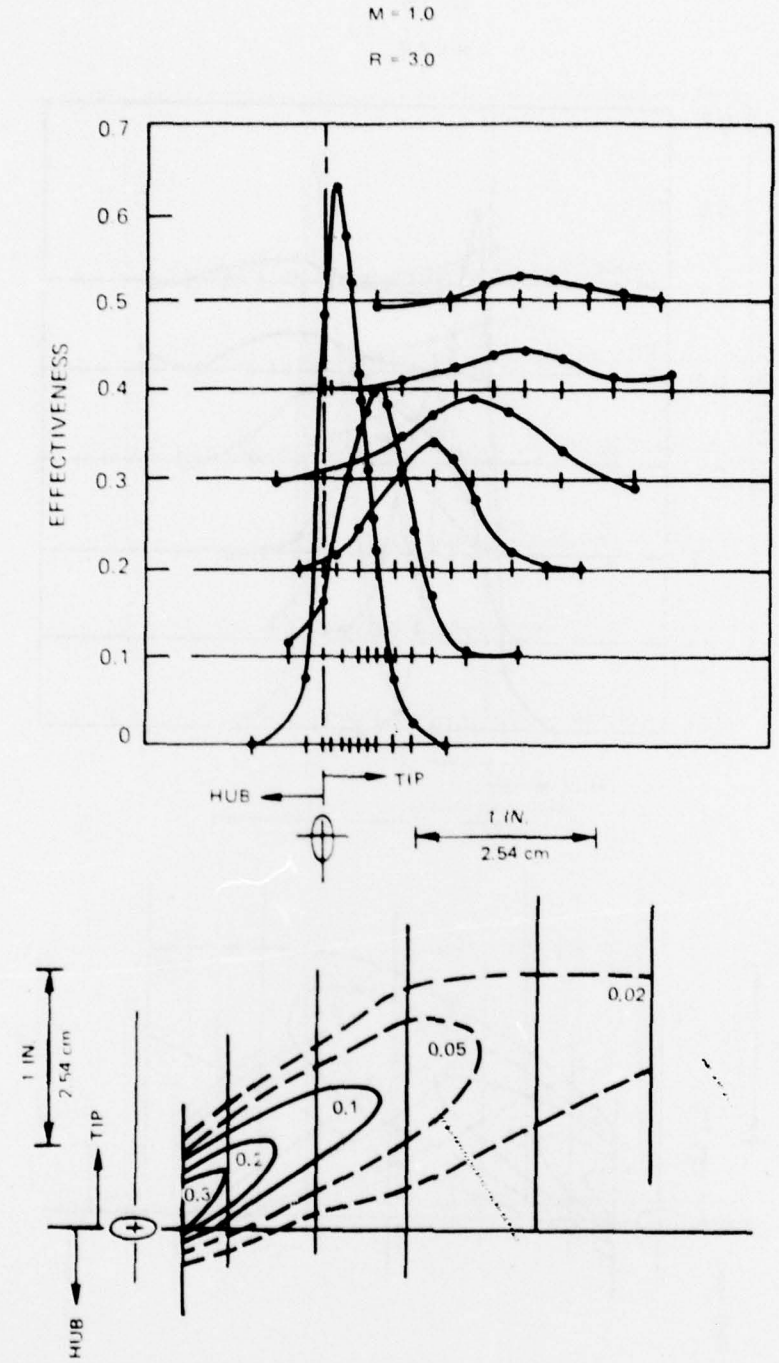

Figure 34. Pressure Surface Film Cooling, M = 1.0, R = 3.0

78-06-31-7

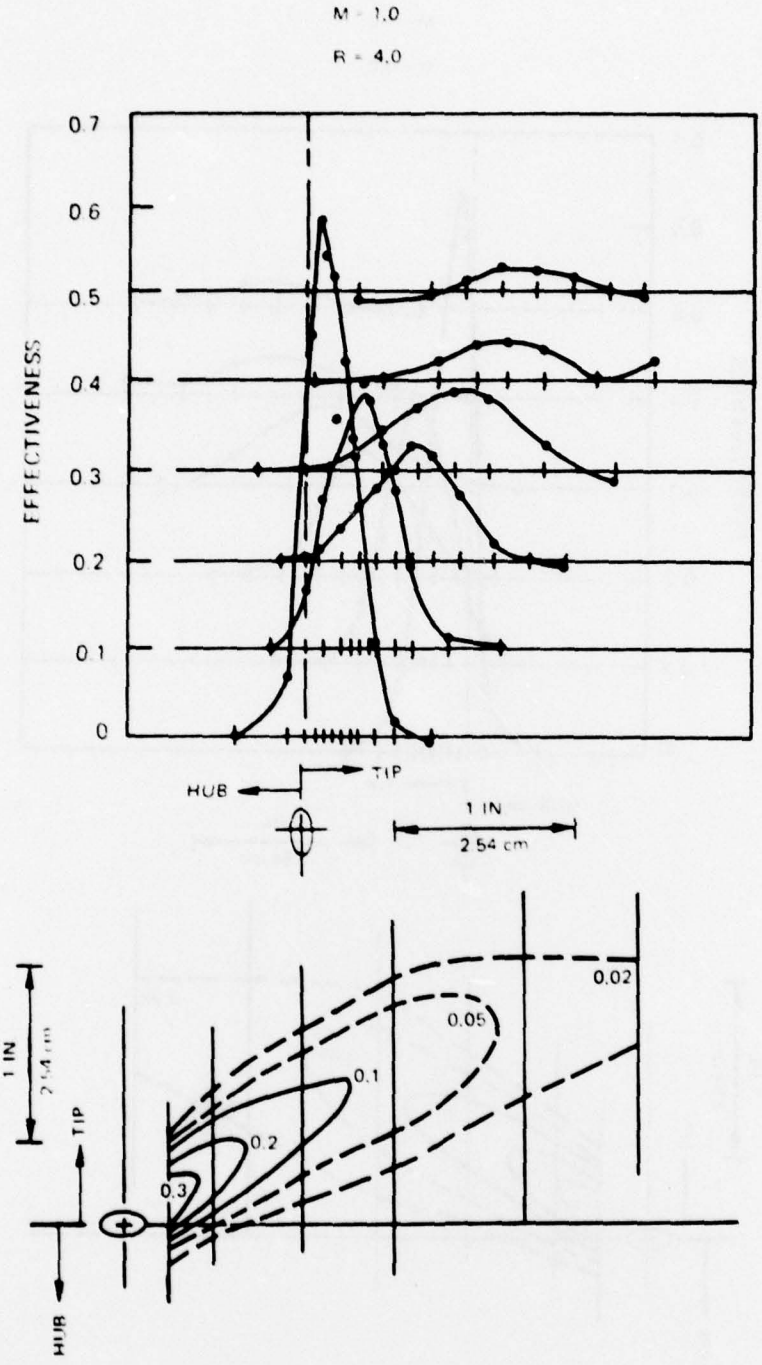

Figure 35. Pressure Surface Film Cooling, M = 1.0, R = 4.0

78 06 31 9

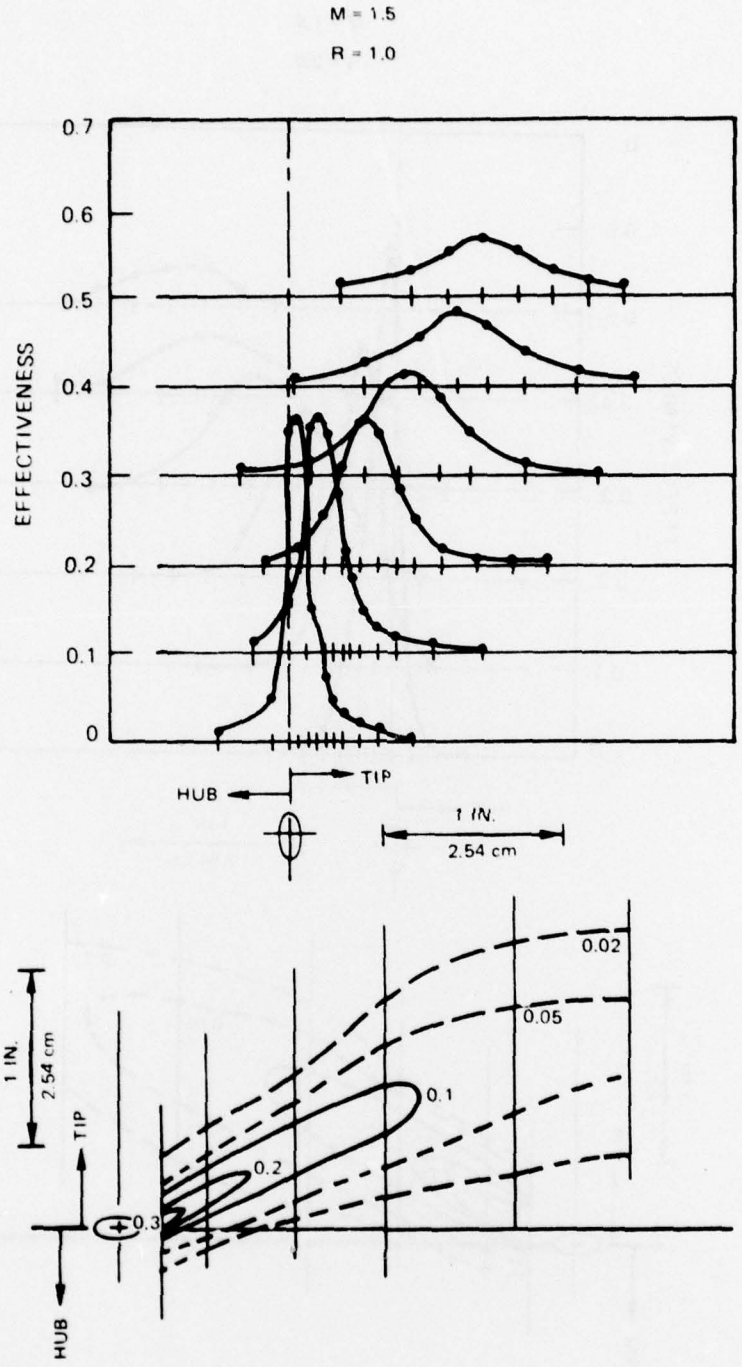

Figure 36. Pressure Surface Film Cooling, M = 1.5, R = 1.0

78-06-31-5

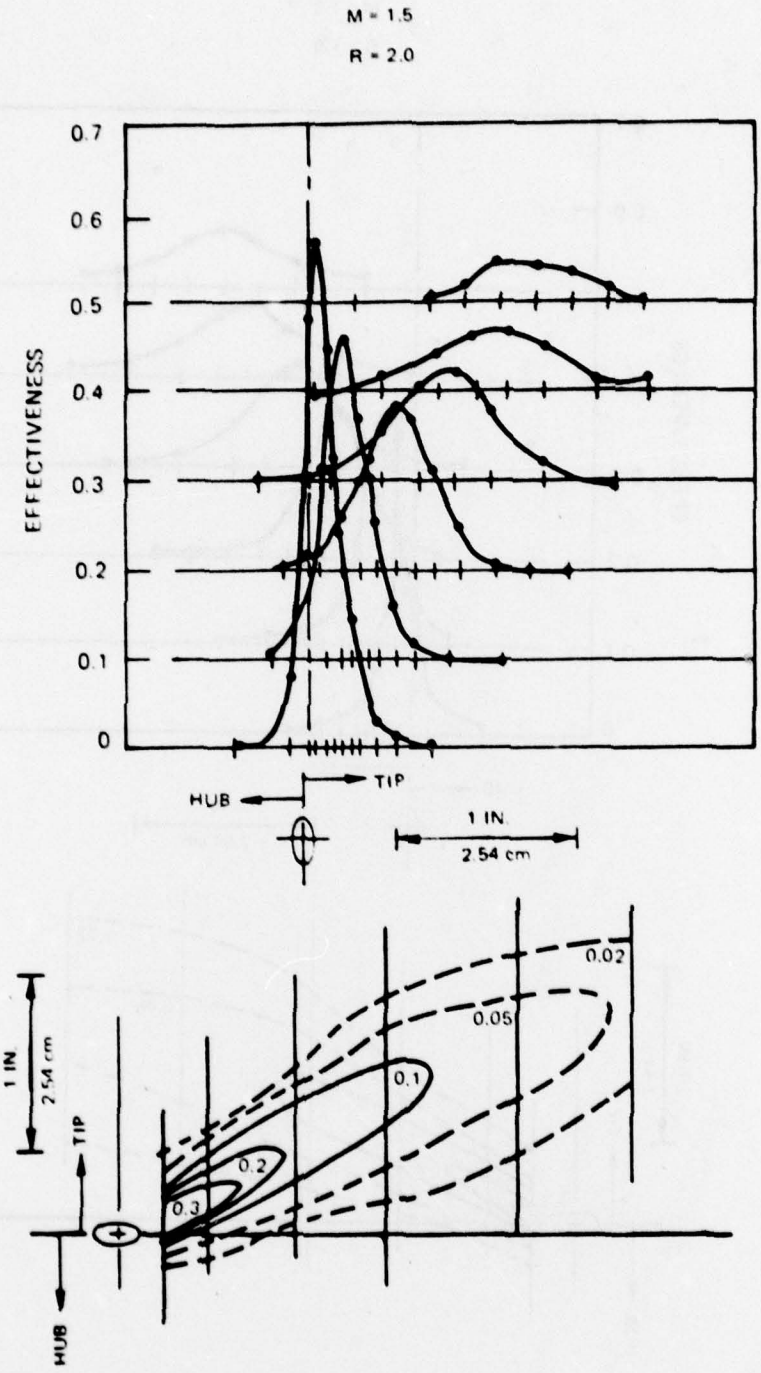

Figure 37. Pressure Surface Film Cooling, M = 1.5, R = 2.0

78-06-31-6

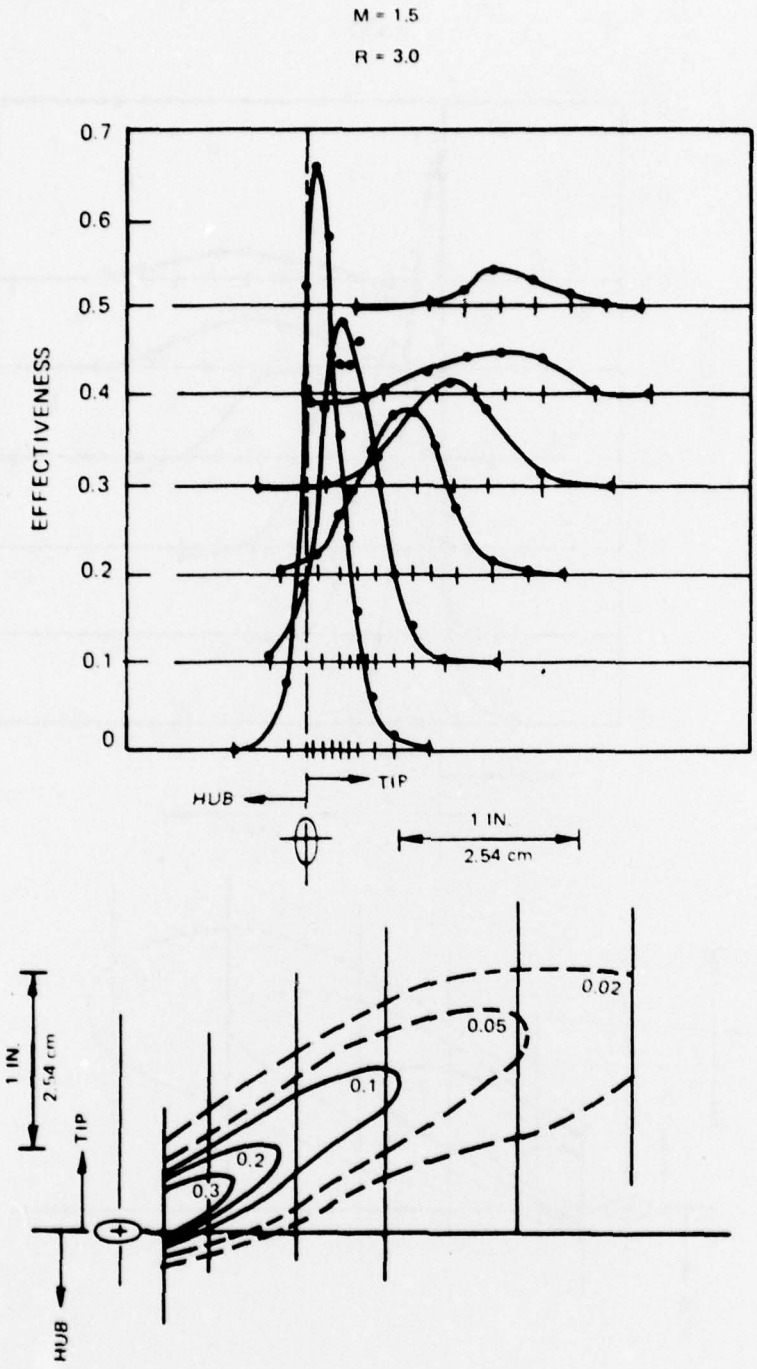

Figure 38. Pressure Surface Film Cooling, M = 1.5, R = 3.0

78-06-31-7

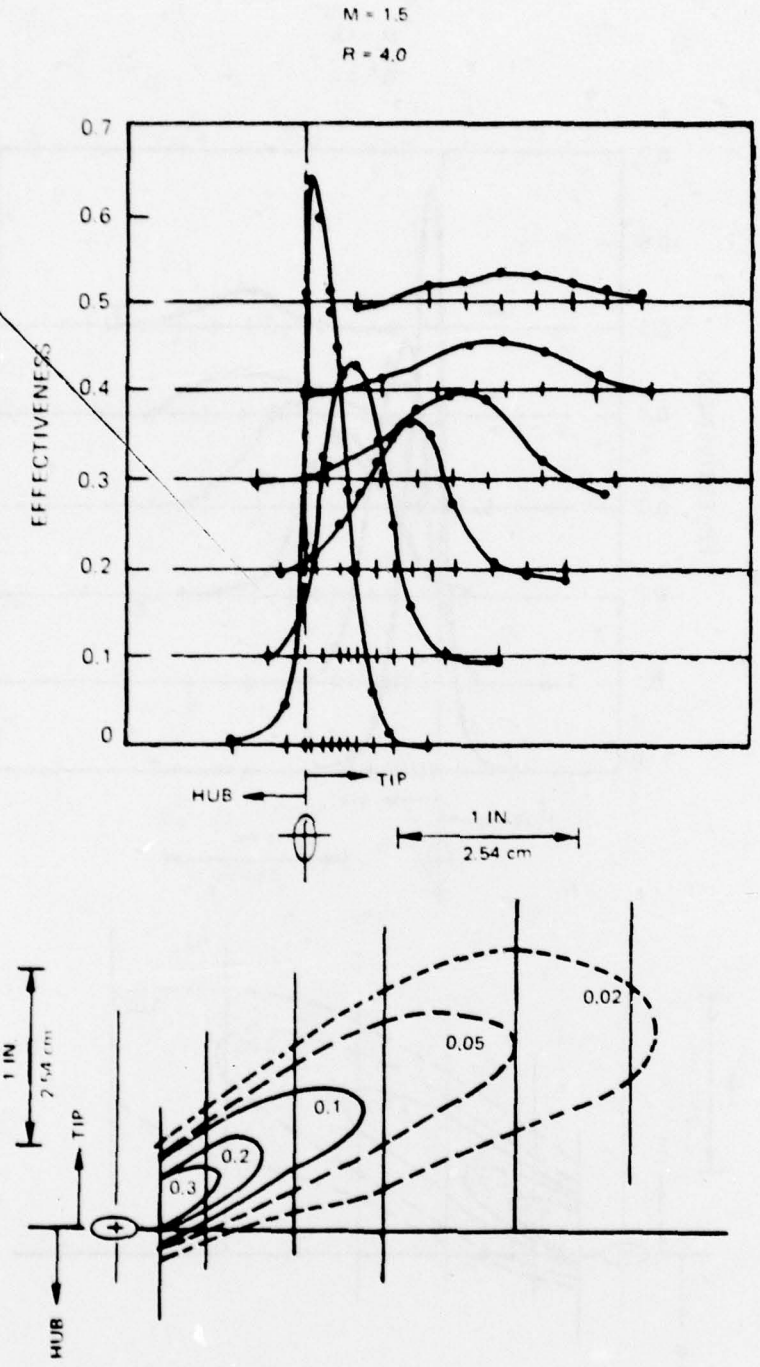

Figure 39. Pressure Surface Film Cooling, M = 1.5, R = 4.0

78-06-31-4

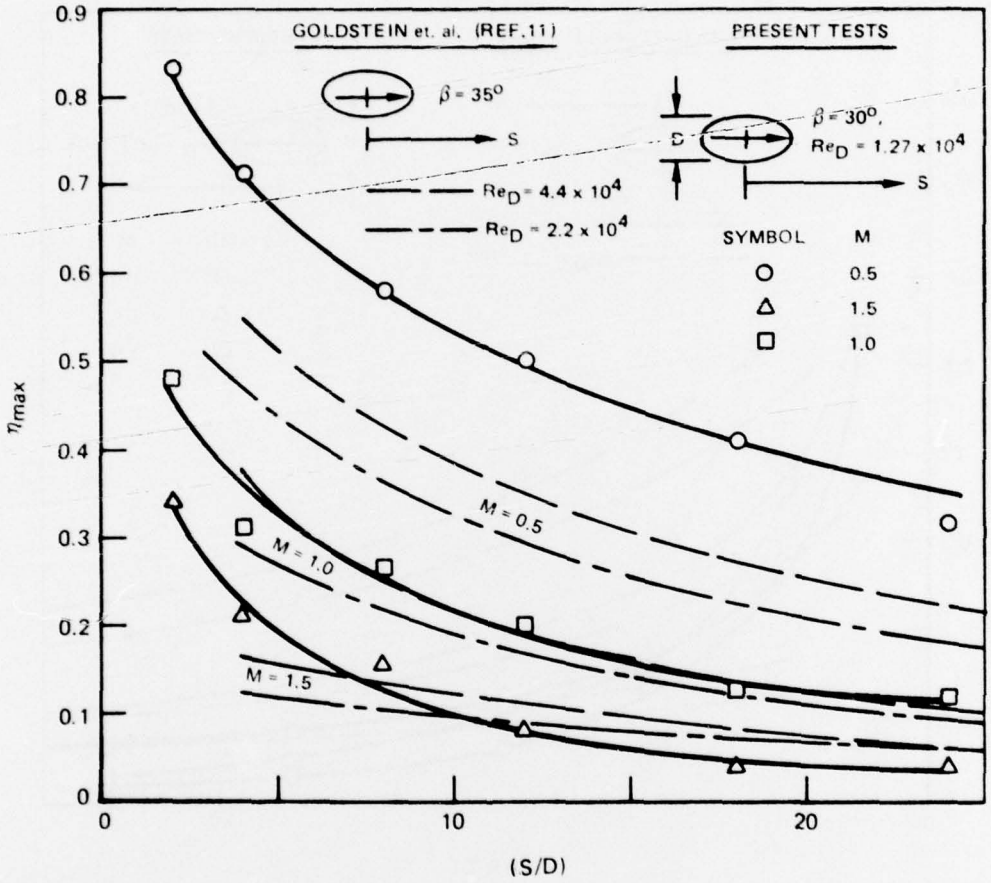

Figure 40. Decay of Maximum Effectiveness, Suction Surface, R = 1

78-06-62-2

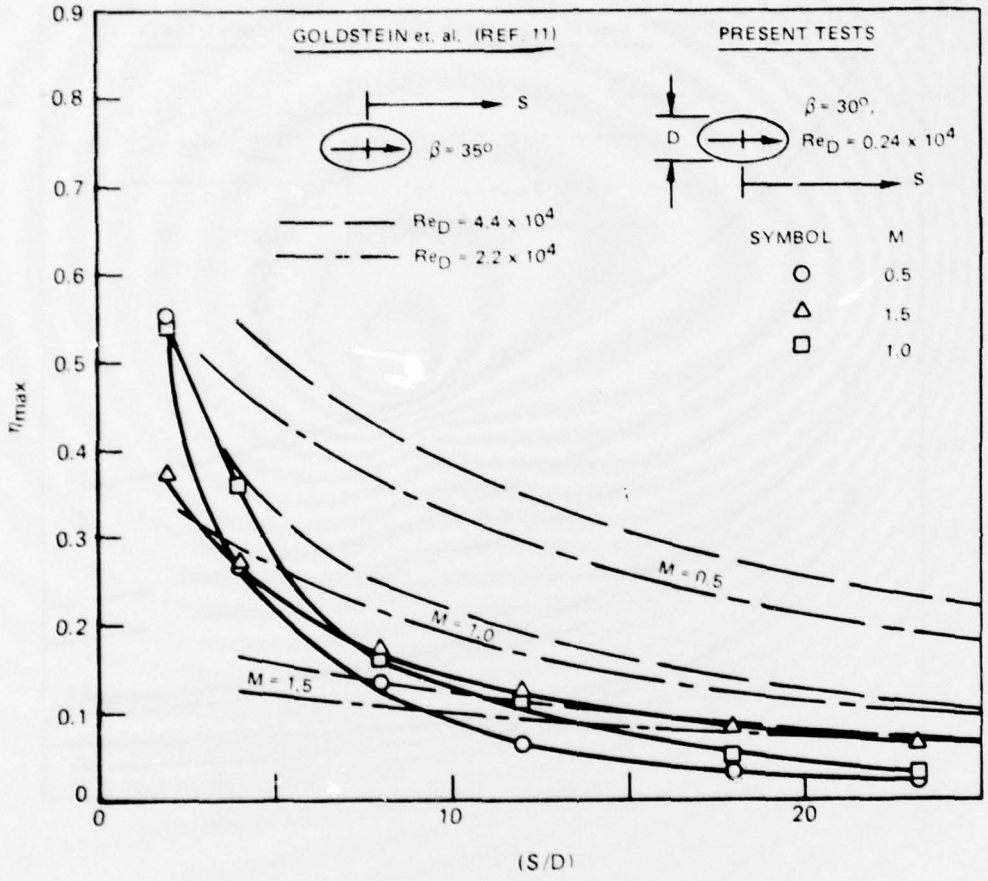

Figure 41. Decay of Maximum Effectiveness, Pressure Surface, R = 1

78-06-62-3

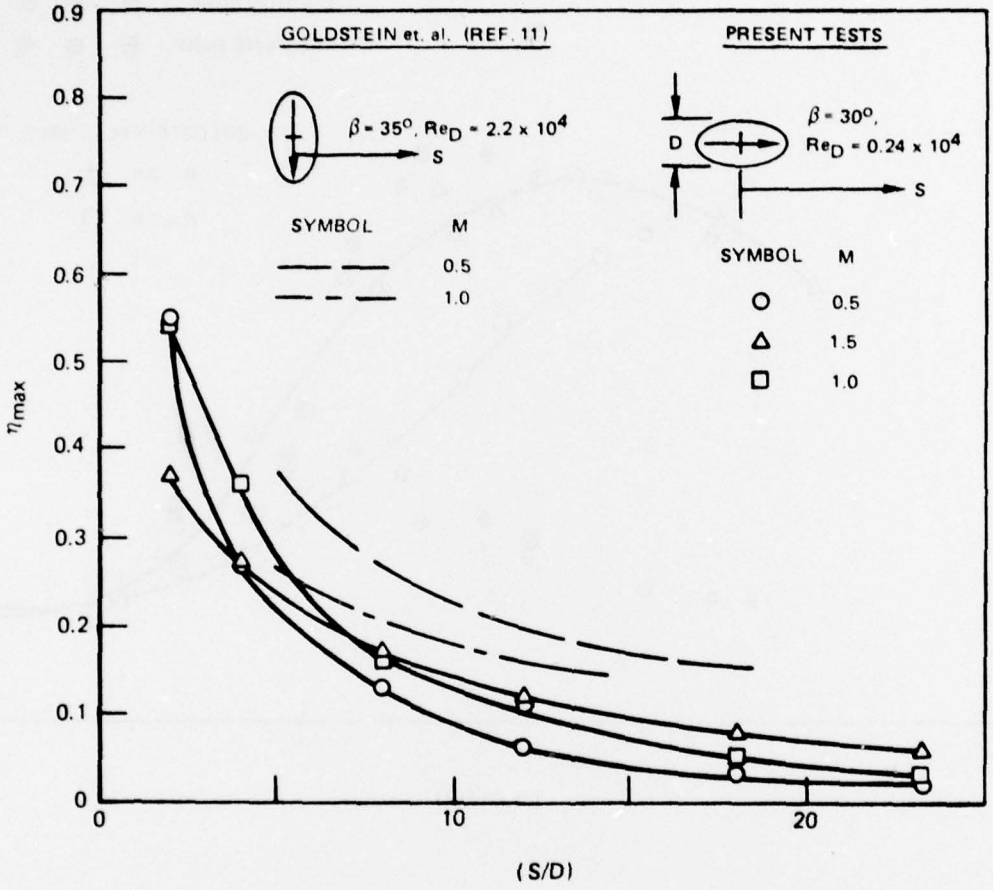

Figure 42. Decay of Maximum Effectiveness, Pressure Surface, R = 1

78-06-62-4

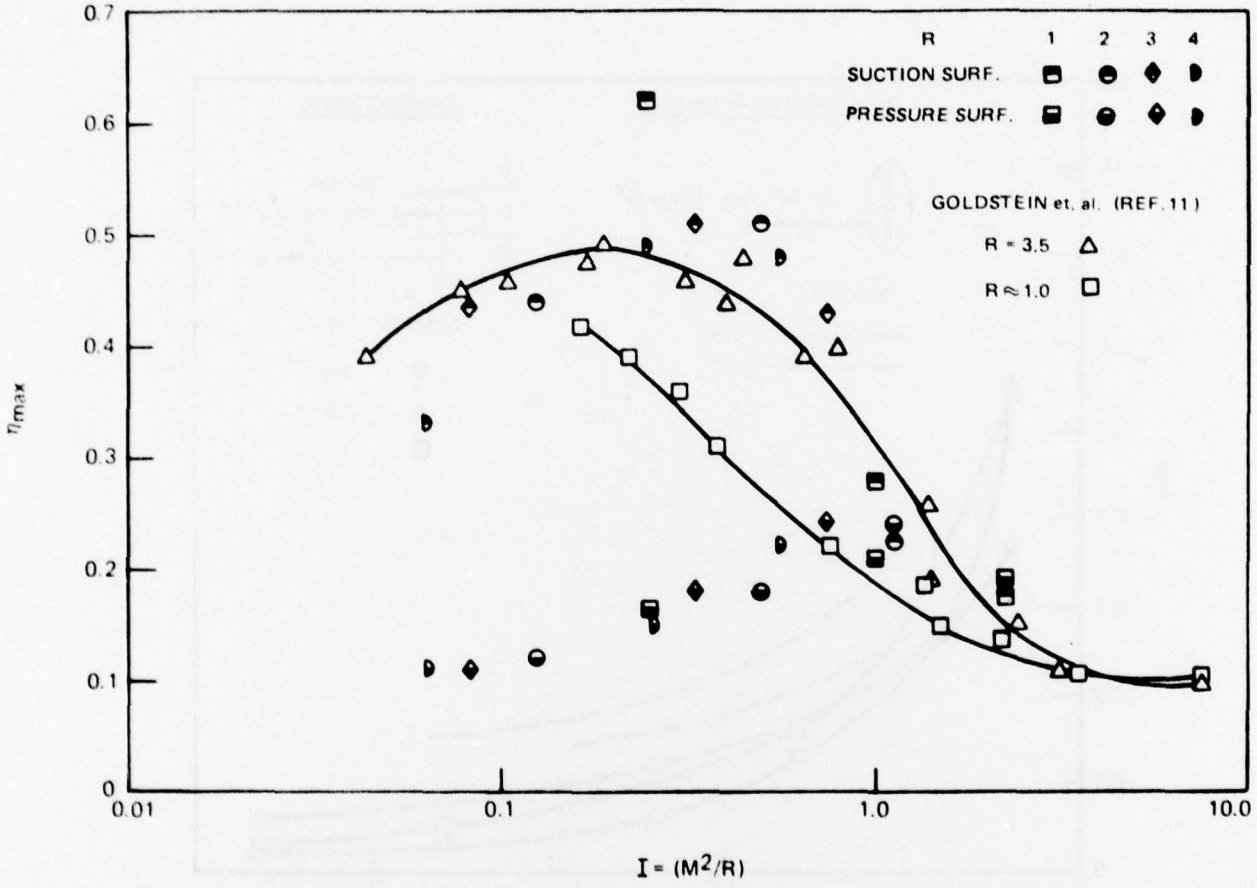

Figure 43. Maximum Effectiveness as a Function of Momentum Flux Ratio and Density Ratio (S/D = 6.6)

78-06-62-1

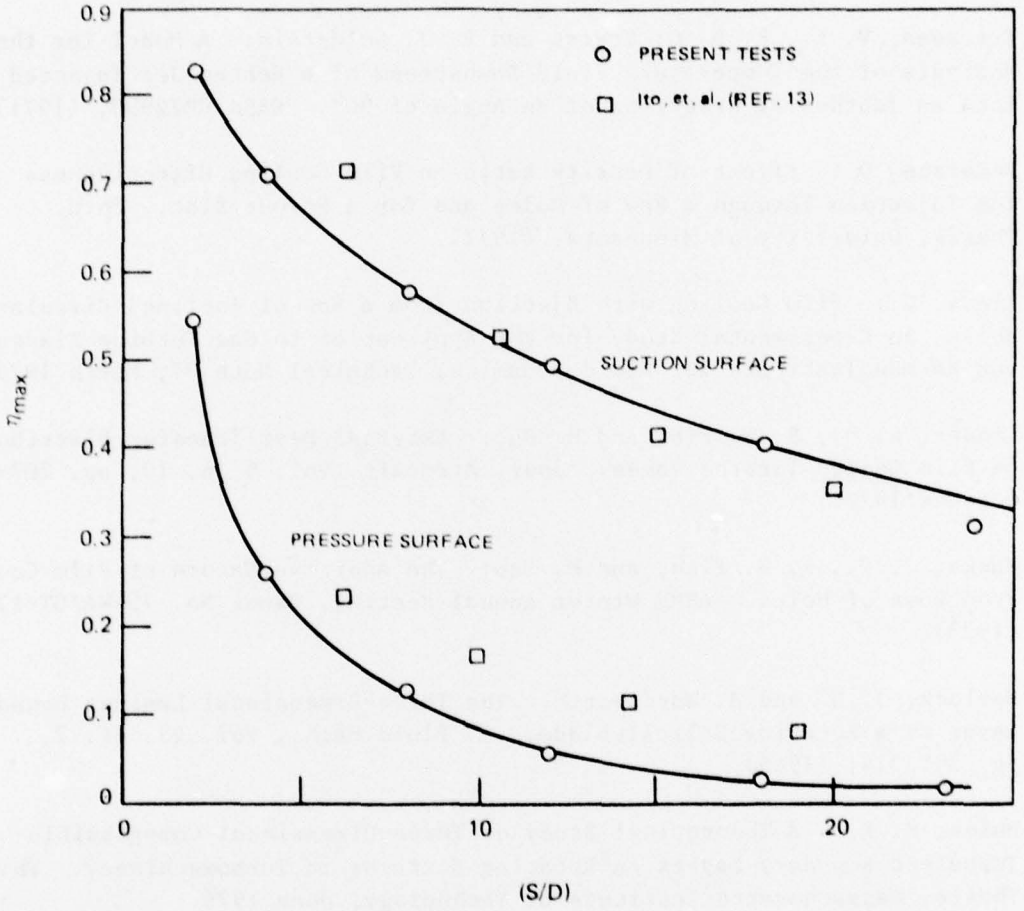

Figure 44. Decay of Maximum Effectiveness, M = 0.5, R ≈ 1

78-07-52-2

REFERENCES

1. Goldstein, R. J.: "Film Cooling" in Advances in Heat Transfer. Academic Press, New York and London, Vol. 7, p. 321, (1971).

2. Ericksen, V. L.: Film Cooling Effectiveness and Heat Transfer with Injection Through Holes. Ph.D. Thesis, University of Minnesota, (1971).

3. Ericksen, V. L., E. R. G. Eckert and R. J. Goldstein: A Model for the Analysis of the Temperature Field Downstream of a Heated Jet Injected into an Isothermal Crossflow of an Angle of 90°. NASA CR72990, (1971).

4. Pedersen, D.: Effect of Density Ratio on Film Cooling Effectiveness for Injection Through a Row of Holes and for a Porous Slot. Ph.D. Thesis, University of Minnesota, (1972).

5. Liess, C.: Film Cooling with Ejection from a Row of Inclined Circular Holes, An Experimental Study for the Application to Gas Turbine Blades. von Karman Institute for Fluid Dynamics, Technical Note 97, March 1973.

6. Lander, R. D., R. W. Fish and M. Suo: External Heat Transfer Distributions on Film Cooled Turbine Vanes. Jour. Aircraft, Vol. 9, n. 10, pp. 707-714, October 1972.

7. Muska, J. F., R. W. Fish, and M. Suo: The Additive Nature of Film Cooling From Rows of Holes. ASME Winter Annual Meeting, Paper No. 75-WA/GT-17, (1975).

8. Horlock, J. H. and J. Wordsworth: The Three-Dimensional Laminar Boundary Layer on a Rotating Helical Blade. J. Fluid Mech., Vol. 23, pt. 2, pp. 305-314, (1965).

9. Hules, K. R.: A Theoretical Study of Three-Dimensional Compressible Turbulent Boundary Layers on Rotating Surfaces in Turbomachinery. Ph.D. Thesis, Massachusetts Institute of Technology, June 1976.

10. Reynolds, A. J.: The Variation of Turbulent Prandtl and Schmidt Numbers in Wakes and Jets. Int. J. Heat Mass Transfer, Vol. 19, pp. 757-764 (1976).

REFERENCES (cont'd)

11. Goldstein, R. J., E. R. G. Eckert, V. L. Ericksen and J. W. Ramsey: Film Cooling Following Injection Through Inclined Circular Tubes. NASA CR-72612, November 1969.

12. Colloday, R. S. and L. M. Russell: Flow Visualization of Discrete Hole Film. Cooling for Gas Turbine Applications. ASME 75-WA/HT-12, December 1975.

13. Ito, S., R. J. Goldstein and E. R. G. Eckert: Film Cooling of a Gas Turbine Blade. Proc. 1977 Tokyo Joint Gas Turbine Congress, pp. 30-37, May 22-27, 1977.